PHILOSOPHICAL TRANSACTIONS OF THE ROYAL SOCIETY A MATHEMATICAL, PHYSICAL & ENGINEERING SCIENCES

The Tides of the Northeast Atlantic Ocean

D. E. Cartwright, Anne C. Edden, R. Spencer and J. M. Vassie

Phil. Trans. R. Soc. Lond. A 1980 **298**, 87-139
doi: 10.1098/rsta.1980.0241

THE TIDES OF THE NORTHEAST ATLANTIC OCEAN

By D. E. CARTWRIGHT, ANNE C. EDDEN, R. SPENCER and J. M. VASSIE

Institute of Oceanographic Sciences, Bidston Observatory, Birkenhead, Merseyside L43 7RA, U.K.

(*Communicated by H. Charnock, F.R.S. – Received 22 November* 1979)

[Plate 1]

CONTENTS

	PAGE
1. Introduction	88
2. Outline of experimental programme	89
3. Instrumental techniques	91
4. Thermal effects	94
5. Tidal analysis	96
(*a*) General principles	96
(*b*) The reference tides	98
(*c*) Radiational tides	101
(*d*) Analysis of pelagic records	101
6. Shelf-edge tides	102
(*a*) Tidal currents	102
(*b*) Pressure gradients	104
(*c*) Power flux	106
(*d*) Numerical model for Shetland seas	110
(*e*) Diurnal anomalies	112
7. Ocean tides	114
(*a*) East–west profiles	114
(*b*) Comparison with computed tides	115
(*c*) Cotidal maps–diurnal	117
(*d*) Cotidal maps–semi-diurnal	120
(*e*) Currents and power flux	121
(*f*) Tests for mass continuity	128
(*g*) Cotidal map for M_3	128
8. Concluding remarks	130
Appendix A. Harmonic constants from pelagic stations	131
Appendix B. Harmonic constants from relevant shore stations	134
Appendix C. A conjugate pair of filters for tidal and other purposes	137
References	138

Vol. 298. A 1436. 11 [Published 30 August 1980

The results of a ten-year programme of measurement and analysis of the tides in the open sea west of Europe are described. Instrumental techniques were developed during the period from capacitance-plane sensors used in shelf seas to strain-gauges and quartz crystal sensors used in oceanic depths up to about 4 km. The measuring stations form two chains, one on the edge of the shelf surrounding the British Isles, and the other surrounding an oceanic area bounded by Scotland, Iceland, the Azores and South Portugal, which is subdivided by a line of stations along the $53\frac{1}{2}°$ parallel from Inishbofin to the mid-Atlantic Ridge. Records from tide gauges at strategic oceanic sites were collected and analysed over long periods to provide a basis for accurate analysis of the relatively short-term pelagic pressure records. Tidal admittances to the generating potential vary smoothly over the region except for a change in the age (phase slope) of the diurnal tides towards Reykjavik.

The shelf-edge chain included current meters, enabling a direct estimation of the M_2 power transmission on to the shelf, namely 60 GW between Malin Head (Eire) and Florø (Norway) and 190 GW between Valentia (Eire) and the Brittany coast near Ouessant. When combined with known power fluxes into the Irish Sea and through the Dover Strait, these give figures for tidal dissipation in the North and Scottish seas that considerably exceed direct estimates based on bottom friction, confirming similar results by Robinson (1979) for the Irish Sea. Dissipation in the English Channel and western Celtic Sea is also much greater than was assumed by Miller (1966). Further, when the eastward flux of energy out of the ocean is computed solely on the basis of the cotidal map drawn for M_2 it is found that about 360 GW is fed into the shelf region between Lisbon and Valentia Island, indicating a substantial loss along the Biscay shelf south of Ouessant. Thus, all estimates of energy loss in the region studied greatly exceed previously assumed values. Dissipation within the main oceanic area itself is, however, about as small as expected.

The diurnal tides in the shelf zones are considerably unlike Kelvin-waves, having short wavelength variations and a tendency for larger amplitudes on the open shelf than at the coast. This probably results from the presence of shelf-wave modes previously identified only in the region of St Kilda. The semi-diurnal tides however have much more regular behaviour along the shelf, with a Kelvin-wave profile west of Inishbofin.

The tidal constants at two representative oceanic sites are compared with estimates from recent computational models, with wide ranges from fair agreement to disagreement, showing that tidal computations for the North Atlantic are not so uncontroversial as is often supposed. Avoiding reliance on computational modelling, the authors present cotidal maps of plausible accuracy for the constituents O_1, K_1, M_2, S_2 and M_3. Currents and power fluxes calculated from the M_2 map are presented and discussed.

The principal oceanic amphidromes for the diurnal and semi-diurnal tides are west of the area studied, but their positions are estimated reliably. A major semi-diurnal amphidrome east of Iceland is confirmed, but there is no evidence for a supposed amphidrome centred on the Faeroe Islands. The cotidal map for M_3 is the first ever produced for an oceanic area. It contains two amphidromes near the mid-Atlantic Ridge.

1. Introduction

Intrinsic knowledge of the oceanic tides advances more slowly than the several geophysical disciplines that now require it. The situation is epitomized by the recent convergence of estimates of the total dissipation in the M_2 tide, by the use of astronomical techniques, to about 3.5×10^3 GW (Lambeck 1977), while oceanographers are still unable to identify any physical sink of energy which could account for more than Miller's (1966) estimate of 1.7×10^3 GW. The recent removal of the Bering Sea from the usual list of areas of major shallow-water dissipation (Sündermann 1977) widens the gap between geophysical and oceanographic understanding of the tides still further.

PHILOSOPHICAL TRANSACTIONS OF THE ROYAL SOCIETY A MATHEMATICAL, PHYSICAL & ENGINEERING SCIENCES

Some twenty years ago, two new techniques emerged that promised between them to solve all outstanding tidal problems. They were the numerical treatment of Laplace's tidal equations (L.t.e.) on a global scale by large computers, and the direct measurement of oceanic tides by sea-bed pressure recorders. Many cotidal maps have since been produced, at least for the M_2 tide, by numerical solution of L.t.e. with various physical constraints (Hendershott 1977). But while the solutions agree in some major features there are too many points of disagreement for any one to be accepted as 'correct'. The recent solutions that allow for elastic distortion of the Earth's crust and the self-attractions of tidal bulges (for example, Accad & Pekeris 1978, Parke & Hendershott 1979) mark an important advance in technique and improvement in realism, but there are still considerable differences between their results and direct measurements. The basic difficulties appear to be the closeness to resonance of some ocean basins such as the Atlantic, and the lack of accurate knowledge of the nature and regional distribution of the energy sinks. It is true that even the published solutions for a rigid Earth somehow contrive to give realistic figures for the acceleration of the Moon's longitude (Lambeck 1977), but this can hardly be said to be an adequate sole criterion for the accuracy of a cotidal map.

Direct pelagic tidal measurements would seem to be the obvious complement to such computer experiments, but the two sorts of activity have been conducted rather independently, by different groups of scientists. The few designers of deep-sea pressure recorders have taken isolated records where ships were available, for example Eyriès *et al.* (1964) in the Bay of Biscay, Filloux (1971) off California, Irish & Snodgrass (1972) south of Australia; Snodgrass *et al.* (1975) in the M.O.D.E. area of the northwest Atlantic. Except for the dynamical synthesis of the recorded tides off California by Munk *et al.* (1970), these measurements have made little impact on numerical modelling procedures. In 1971 the S.C.O.R./I.A.P.S.O./Unesco working group no. 27 on 'tides of the open sea' (Scientific Committee for Oceanic Research 1972) recommended six geographical positions where measurements would be of greatest benefit to numerical tidal modellers.† Unfortunately, they were all rather remote from tidally equipped oceanographic institutes, and no record has yet been taken from any of these positions. The main object of the work described in the present paper was, in briefest terms, to remedy this lack of coordination between numerical modellers and sea-going instrument technologists for improving knowledge of the oceanic tides.

2. Outline of experimental programme

The work described completes a phase of a programme of pelagic tidal measurements started by the senior author (D.E.C.) about ten years ago. The main object has been to define the tides unambiguously in a sizeable area of ocean, easily accessible by U.K. research ships but large enough to contain dynamic features relevant to computation of tides on a global scale. The scale of the concept has grown progressively as measuring facilities at I.O.S. have widened through a parallel programme of instrumental development.

The original concept embraced only the edge of the continental shelf surrounding Britain. The technique for recording pressure variations in depths less than 200 m is easier than at oceanic depths, and the tides on the outer shelf were just as unknown as in the ocean. Shelf-edge measurements could serve as boundary conditions both for oceanic computer models, looking outwards, and for tidal and storm-surge models covering the shallow seas looking inwards. An

† An extended set of test points has recently been proposed by Parke (1979).

PHILOSOPHICAL TRANSACTIONS OF THE ROYAL SOCIETY A MATHEMATICAL, PHYSICAL & ENGINEERING SCIENCES

important factor to determine was the flux of tidal energy into the shelf seas, equated to the total dissipation there, and this required the long-term measurement of current, which was already an established technique in 1968.

Another early task was to determine the tidal characteristics at outlying isles such as Hirta (St Kilda), Foula and Unst (Shetland) and Inishbofin and Valentia (Eire), where lack of shipping interests caused neglect in official tidal records. Our very first tentative efforts, using a crude pneumatic recorder at St Kilda and some current meters moored along 100 km of the local shelf, revealed an unsuspected phenomenon in the diurnal tides. It is the only recorded case of a diurnal continental shelf-wave, with strong associated currents (Cartwright 1969; Cartwright *et al.* 1980). This added to our confidence that we were by no means beating over well-known grounds.

Our technique for tidal pressure recording in shelf depths developed during 1969–72 (Collar & Spencer 1970; Gwilliam & Collar 1974, U.K. Inst. Oceanogr. Sci., rep. no. 14 – unpublished), while we managed to take useful records along the northern British shelf at about 100 km spacing between Malin Head (Eire) and Florø (Norway) with special attention to detail around the Shetland complex. A general survey of the records by Collar & Cartwright (1972) showed them to be repeatably accurate, low in noise content and containing negligible high harmonic distortion of the tides. (A peculiar 6th harmonic appearing north of Shetland (Cartwright & Young 1974) was an isolated curiosity rather than a regular feature.) Details of the resulting tidal constants from the northern shelf were set out by Cartwright (1976*a*).

Our adaptation of a 'Bell and Howell' strain-gauge for use as a deep-sea tidal pressure sensor (Gwilliam 1976), was first applied seriously at 1200 m in the Faeroes–Shetland channel during the I.C.E.S. 'Overflow' exercise in the summer of 1973. The sub-zero temperatures of the Arctic bottom water caused problems with the acoustic release sensitivity on our first attempt at recovery of this, our prototype deep capsule, the permanent loss of which might have put an end to our oceanic tidal programme. However, it was recovered in November 1973 during a brief lull between two storms,† enabling us to re-deploy it, as well as two of the I.O.S. shelf capsules, in the 'Intercalibration Exercise' off the Brittany shelf organized by S.C.O.R./I.A.P.S.O./Unesco working group no. 27, (Spencer & Gwilliam 1974; Unesco 1975).

Equipped with both shelf capsules and deep-water pressure capsules viable to 4000 m, we were able to plan cruises in which the shelf capsules were deployed along the tidally important shelf-edge between southwest Ireland and Brittany, on the way to oceanic areas further to the south and west. We planned to surround areas of ocean of order $20° \times 20°$ by a circuit of tidal measurements that would enable the tides in their interior to be determined by numerical solution of L.t.e. or otherwise – a procedure suggested by Hansen (1966). Unlike the Atlantic coast of the British Isles, the Atlantic coasts of France, Spain and Portugal have narrow shelves, so that their known shore-based tidal records adequately represent the ocean boundary. Use was made of island stations such as the Azores and seamounts such as 'Josephine' and 'Ormonde' that were shallow enough for our shelf capsules. The Biscay and Iberian abyssal plains were mostly deeper than our 4000 m limit, but the mid-Atlantic Ridge provided ample scope, and it was possible to find suitable sites along east–west lines between Cabo São Vicente and the Azores and from our shore installation at Inishbofin off Connemara to the Ridge at 30° west. The tides in mid-ocean change more slowly with distance than in the wider shelf seas, so spacing of about 400 km or four degrees of latitude was deemed sufficient. We did not measure currents at the deep stations because of the difficulty of resolving the internal modes.

† For this recovery operation we are particularly indebted to our colleague Dennis Gaunt.

PHILOSOPHICAL TRANSACTIONS OF THE ROYAL SOCIETY A MATHEMATICAL, PHYSICAL & ENGINEERING SCIENCES

The south-western shelf-edge circuit was completed in 1976, and nearly all of the Cabo São Vicente–Azores–Inishbofin oceanic circuit in early 1977. The only missing point was D7 at 53½° N, 30° W, our only case of non-recovery of a deep capsule. (Shelf capsules were not infrequently damaged or moved by trawlers but were sometimes brought into and recovered from a fishing port.) D7 was re-laid and successfully recovered in late 1977, when the opportunity was also taken to close a circuit north of the Inishbofin parallel following the Reykjanes Ridge to Iceland and including an additional station between southeast Iceland and the Faeroes, linking with our earlier northern shelf stations. To help tidal definition along the south Icelandic shelf, the Icelandic Hydrographic Service gave us extensive records from their tide gauge at Reykjavik and allowed us to install our own recorder for a year well exposed to deep water at Djupivogur, a small fishing port on the southeast coast.

Wherever possible, stations were occupied for at least a lunar cycle of 28–30 d, but sometimes cruise planning or instrumental defects limited records to 15 d or (rarely) less. Planning ship-time for such operations is a fairly serious matter because of its high cost and the need to occupy the time between laying and recovery of the capsules usefully. Usually, we found another oceanographic group interested in working in the area. Sometimes we made use of 'ships of opportunity' going to other areas, on which a capsule could be laid on the way out and recovered on the way back. By counting laying and recovery operations as occupying a single 'cruise', the 37 successful pressure stations and 20 current stations which form the basis of this paper took 10 cruises of ships from the N.E.R.C. research vessel fleet. Most often, we used R.R.S. *Discovery*, but some of the earlier, shallow-water work was done on the research vessels *John Murray*, *Shackleton* and *Surveyor* (chartered from the 'Gard Line').

A map of all sites occupied is shown in figure 1, and their positions, depths and times of recording are detailed in appendix A.

3. Instrumental techniques

Enough references to published descriptions of successive phases of our instrumental development have been given above to make it unnecessary to go into great detail here. We shall merely outline the main features and elaborate a little on thermal effects.

Overall, our technique for recording pressure variations at the sea bed is similar to that used by others and only a little less refined than the sophisticated system developed by Snodgrass (1968). A buoyant assembly (figure 2*a*, plate 1), consisting of pressure- and temperature-sensors, chronometry, counting circuits, digital magnetic tape, acoustic beacons and electric power cells, is attached to a ballast frame through a pyrotechnic link which can be fired on acoustical command from the surface, causing the main assembly to rise for recovery. Our ballast frames consist of a fabricated-steel flat tripod weighing about 60 kg in water, and the buoyancy of the main assembly is about 15 kg. Rates of (free) descent and ascent are in the order of 1 m s^{-1}. In the 'Mark 3' capsule illustrated in figure 2*b*, which was used for most of the deep stations, the main buoyancy is supplied by a forged aluminium sphere (two hemispheres with O-ring seal), 0.7 m diameter, 10 mm wall thickness, containing a bulky but reliable digital tape recorder manufactured by 'Normalair–Garrett', computer circuits and batteries. We have also used fibreglass spheres, but have found that the bonded seals on their cable-entry ports tend to leak slightly. In our latest, 'Mark 4' capsules (figure 2*c*), used, for example, at sites M4 and R3, a miniature 'Sea-data' cassette recorder and low power-consumption integrated circuits allow a 1 m long aluminium

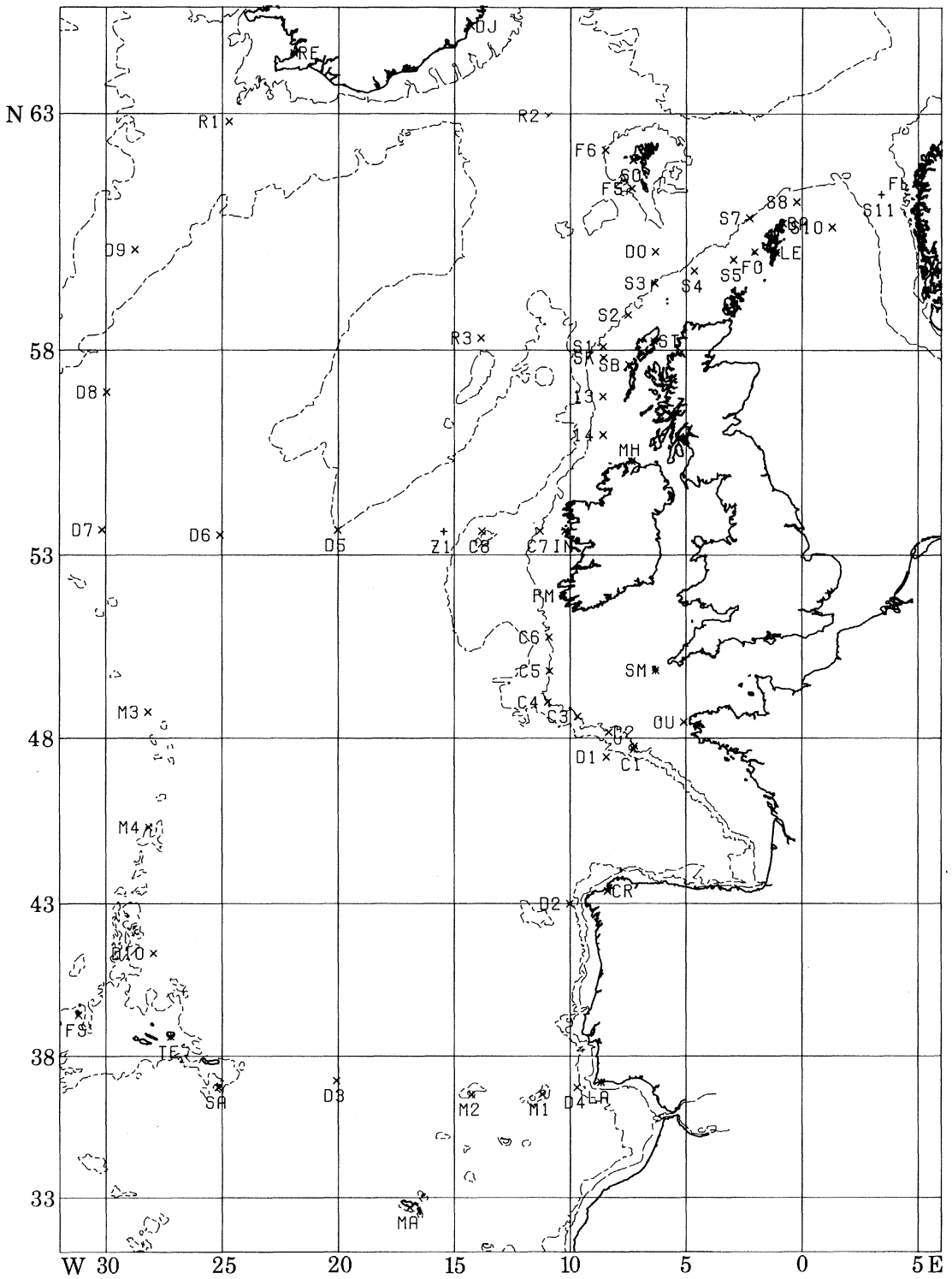

FIGURE 1. Map showing bathymetry and positions of principal tidal stations. Depth contours are 100 and 1000 fm (183 and 1829 m). Numbered stations are pelagic, with constants listed in appendix A. Positions indicated by letters only denote coastal and island sea level stations with constants listed in appendix B.

PHILOSOPHICAL TRANSACTIONS OF THE ROYAL SOCIETY A MATHEMATICAL, PHYSICAL & ENGINEERING SCIENCES

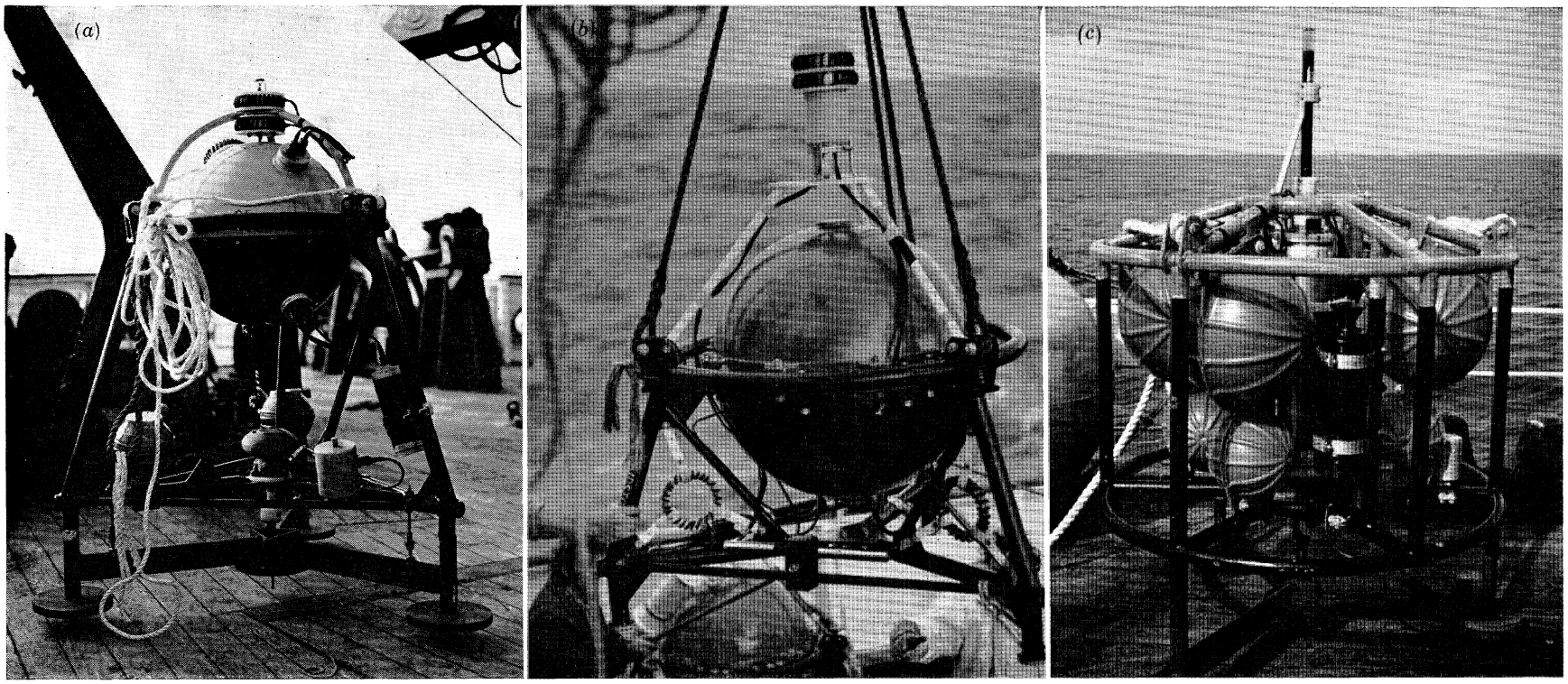

FIGURE 2. The three principal designs of sea-bed pressure capsule. (*a*) The original (mark 1) shelf tide recorder with buoyant sphere containing batteries and heavy data-logger; ellipsoidal unit near centre is capacitance-plate sensor; cylindrical unit nearby houses early strain gauge; toroidal scrolls are acoustic transducers; bottom frame is ballast attached by rapidly corrodible links (side) and acoustic/pyro-release link (centre). (*b*) 'Mark 3' deep capsule, without ballast frame when photographed. Components similar to mark 1; horizontal bar, centre, houses a quartz crystal sensor (not always included); a strain gauge unit is just visible to its left. (*c*) 'Mark 4' deep capsule with lightweight 'Seadata' cassette recorder and computer circuits inside central cylinder. Black cylinder off-centre is ceramic acoustic transducer; strain-gauge sensors are attached to the lower part of the frame; double-action release link attached centrally above ballast frame; main buoyancy provided by 'Corning' glass spheres in ribbed protective casings; the topmost cylinder is a flashing light for surface recovery at night.

(*Facing p.* 93)

alloy tube of 0.15 m internal diameter and 15 mm wall thickness to be used to house these units. The main buoyancy is supplied by the addition of 'Corning' glass spheres mounted in the tubular framework.

Our acoustic recovery system is that developed over several years at the I.O.S. (Wormley) laboratories (Harris, M. J. 1973, U.K. Inst. Oceanogr. Sci. (N.I.O.) Internal rep. no. A61). 'Pingers' of precise repetition rates of order 1 s are turned on or off by a 10 kHz acoustic carrier wave frequency-modulated at set tones in the range 300–600 Hz. In the 'release-pinger' mode, the transmitted signal must persist for at least 100 s before the pyro-release link is fired. The mechanical release-link can be activated by either of two alternative acoustic systems, for security. The acoustic transponders are nickel scrolls or ceramic resonators. In present practice, each capsule carries two 'release-pinger' systems and two 'command-pinger' systems that act as homing beacons. Acoustic contact is usually good within 5 km horizontal range in deep water, within 2 km in shelf-edge depths. Obviously, modern aids to precise navigation, especially that afforded by the 'Transit' Doppler satellites, are an essential complement.

Our first sensor for shelf depths was a thick beryllium–copper variable-capacitance plate, devised from a principle used in wave recording (Collar & Spencer 1970). This has always given low noise and drift rate (see, for example, Unesco 1975), but it is heavy and expensive to manufacture. Later models employed special radial-grain forging to give even further reduced drift rate and thermal coefficient. The adapted strain-gauge sensors (Gwilliam & Collar 1974) are cheaper, lighter and more easily reproducible, with quite acceptable noise and drift characteristics, low power consumption and about the same thermal sensitivity as the capacitance plates. They are light enough to allow two sensors on the same capsule, to give greater reliability.

Adaptation of the strain-gauge sensors to oceanic depths required an order of magnitude greater sensitivity to pressure variations relative to ambient pressure and compensation for the natural increase of thermal sensitivity with depth. These were achieved by general improvement of circuit design by using a bridge assembly to convert changes in resistance to changes in frequency, compensating thermal sensitivity of the sensor by thermal characteristics of electrical components and great care in calibration procedures both before and after use (Spencer & Gwilliam 1975; Gwilliam 1976). They have given satisfactory and consistent results and compare well with commercial quartz crystal sensors with very low thermal sensitivity, which we have also added in recent assemblies.

Implicit in the above has been the necessity to record temperature independently to correct the pressure signals for thermal sensitivity. This is important not only to reduce general noise level but also to remove spurious tidal variations from internal tides in thermally stratified water. We have used thermistor beads for the capacitance plate sensors and for monitoring temperature at various points of the capsule. Later, we introduced platinum resistance thermometers using the same type of bridge network as with the strain gauges to convert their change in resistance to modulated frequency. In one case – 'Josephine seamount' 1972 – the temperature sensors failed for obscure reasons, but it was possible to reconstruct the temperature signal by comparing the pressure signals from a capacitance plate and a strain gauge, these two having temperature coefficients of opposite sign.

Nearly all signals were recorded digitally as integrated frequency counts over 890 s periods at 900 s intervals (repetition rate, 4 h^{-1}) except for the Mark 4 assemblies for which the repetition rate was increased to 16 h^{-1}. The effective time of each sample was of course taken to be half the time interval earlier than the instant when it was recorded.

PHILOSOPHICAL TRANSACTIONS OF THE ROYAL SOCIETY A MATHEMATICAL, PHYSICAL & ENGINEERING SCIENCES

4. Thermal effects

It is often thought that thermal noise in the deep ocean is less troublesome than on the shelf. We have not invariably found this to be the case in the northeast Atlantic. Figure 3*a* shows four simultaneous temperature records from the S.C.O.R. 'Intercalibration exercise' in November–December 1973 (Unesco 1975). The lower pair were 8 km apart on the shelf edge at position C1, about 170 m deep; the upper pair were recorded on the same capsule on a terrace at position D1, about 110 km WSW of C1 at a depth of 2160 m. (See figure 1 and appendix A for positions.) The shallow pair are clearly much more noisy, with strong tidal and low frequency

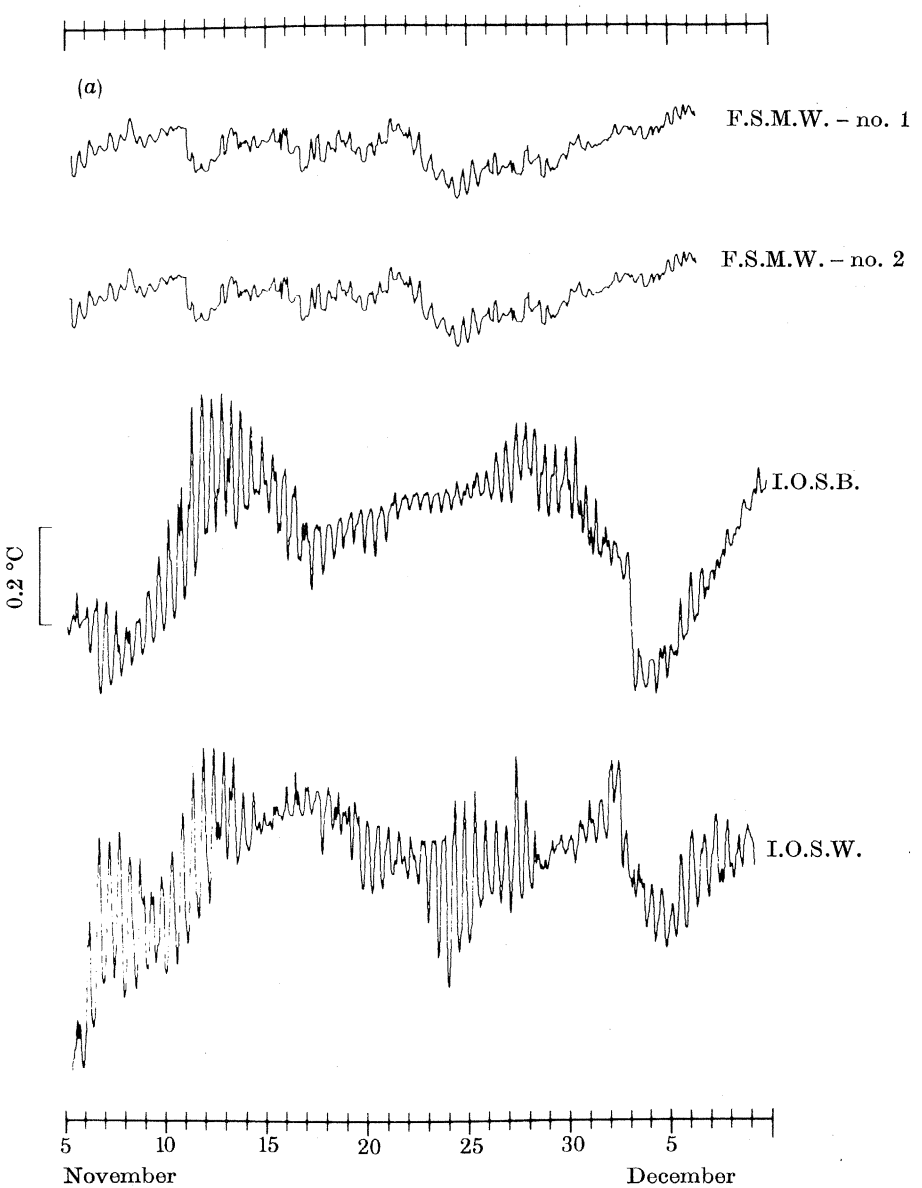

Figure 3(*a*). Simultaneous temperature records from S.C.O.R./Unesco Intercalibration Exercise in 1973. Upper two traces from 'Snodgrass' capsule in 2150 m. Lower two traces from two I.O.S. capsules in about 170 m, 8 km apart, 110 km from deep capsule (from Unesco 1975).

variations of order 0.5 °C. It is interesting that, while the low frequency variations recorded at the two sites were fairly similar, the tidal variations, resulting from internal tides, are very dissimilar at only 8 km separation. The deeper records are qualitatively similar to the shallow records, but the variations are only in the range 0.2 °C. This range is still much greater than in the temperature variations recorded at, typically, 5000 m in the eastern Pacific and in the western North Atlantic (Snodgrass *et al.* 1975), which are all within 0.05 °C.

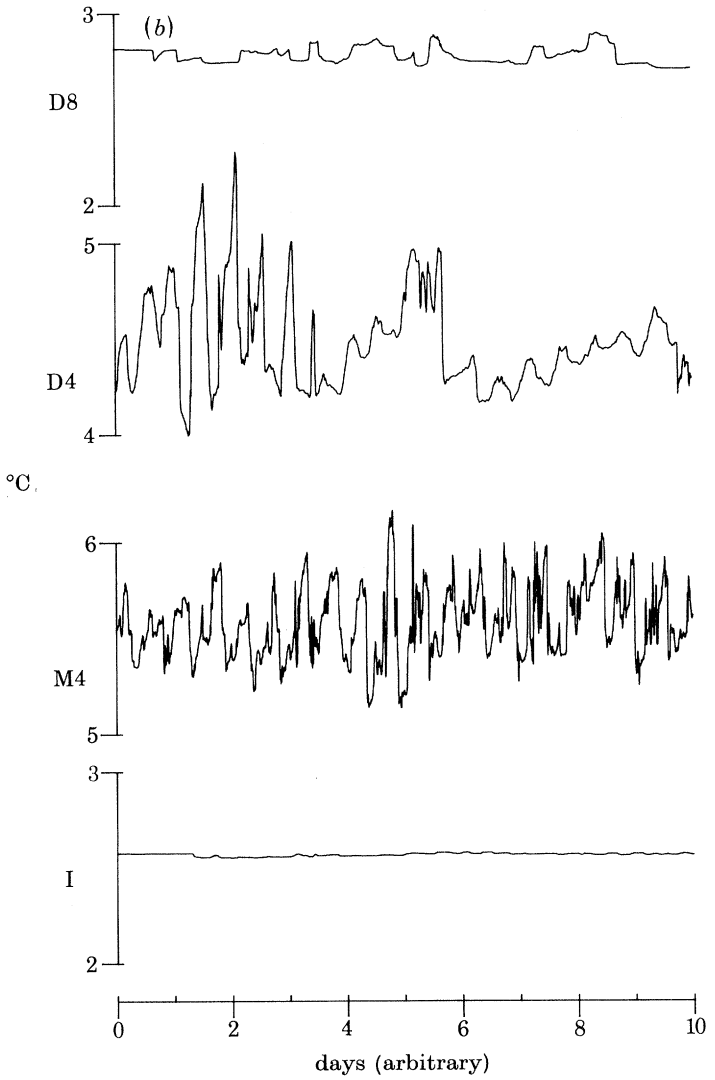

FIGURE 3(*b*). Four contrasting non-simultaneous temperature records from various stations: D8 (2448 m), D4 (1983 m), M4 (1047 m), and a station (3830 m south of C4) I.

Figure 3*b* shows the temperatures at a wider geographical range of deep stations in our area. Ten days are shown for each but the periods are not simultaneous. The bottom trace is from a station 100 km WNW of D1 at a depth of 3830 m the tidal constants of which are not included in this paper. Its variation is in fact within 0.05 °C and it is the quietest we have recorded. The top trace, from station D8 near the mid-Atlantic Ridge at 2448 m, is also fairly quiet, but varies within 0.15 °C. The second trace from the bottom is from M4, a Ridge seamount at 1047 m,

and shows very violent variations within 1 °C, partly tidal and partly at a much higher frequency – this record used a high sampling rate of 16 h^{-1}. The third trace from the bottom, from D4 near the Portuguese shelf at 1983 m, is one of our noisiest deep records, with tidal oscillations and steep frontal drops within a 1.5 °C range. Much of the thermal noise is probably generated by the shelf edge, known to be a source of internal tides (Baines 1974), but the proximity of D4 to the outflow from the Mediterranean is possibly relevant too.

The steep frontal drops in the middle two traces of figure 3*b*, and those that occurred in some other records, caused us difficulty in correcting the strain gauge records for thermal sensitivity. We found in these cases that the thermal response was not instantaneous but had a time-lapse extending over about an hour, owing to differential cooling of various parts of the mechanism. The thermal time-constant of the strain gauge has been shortened by using a 'nylatron' block to insulate it from its case, but for many records affected we found the following type of correction formula was effective

$$p(t) = a + a'(f - \delta f) + a''(f - \delta f)^2 + \ldots,$$

$$\delta f = b_0\,\theta(t) + b_1\,\theta(t - \delta t) + b_2\,\theta(t - 2\delta t) + \ldots,$$

where p is the true pressure in terms of transducer frequency f and a correction δf expressed in terms of the time history of θ, which is the temperature referred to an arbitrary mean temperature. The coefficients a, a', ... are carefully evaluated in a pressure tank, set to the same mean temperature. The coefficients b_m referring to time-lags $m\delta t$ are sometimes determined from laboratory calibrations of a step-response, sometimes from empirical least-squares fitting to the real sea data.

A good example of the necessity for and efficiency of thermal time-lapse correction is shown in figure 4, which depicts the records taken from two pressure sensors and the thermistor during 16 d at R2, 444 m deep, on the Iceland–Faeroe Rise. The temperature trace, near the middle, is very noisy indeed, with a range of nearly 4 °C, associated with overflow of cold Arctic water into the North Atlantic. Above it are the frequency records from a quartz crystal sensor and from a strain gauge. The quartz crystal is very insensitive to temperature and shows an undisturbed tidal record, while the strain gauge record appears drastically distorted by temperature. The two traces below the temperature record show the result of converting both records to pressure units with a 'static' temperature correction (b_0 only). The strain gauge record is much improved but still has noisy patches near times of sharp temperature change. These are finally eliminated in the bottom trace by use of a more elaborate formula for temperature correction as described above. Tidal analysis of this record gave practically identical results to the analysis of the quartz crystal record.

5. Tidal analysis

(*a*) *General principles*

For every pressure record, including those from short-term shore stations, we followed the analysis procedure proposed by Cartwright *et al.* (1969). This procedure is based on the 'response' method of Munk & Cartwright (1966), simplified for oceanic (linear) tidal records of short duration. An artificial tidal signal $\tilde{\zeta}(t)$, closely related to the data to be analysed, is computed for the same time span as the data plus a few extra days to allow for filter convolutions. $\tilde{\zeta}(t)$ is called the 'reference tide'. Three pairs of conjugate filters are applied to the reference tide, each of which passes a band of frequencies covering one of the three resolvable linear tidal 'species'

1, 2 and 3 (i.e. the nearest integral number of cycles per lunar day). The 'real' member of the mth conjugate pair of filters is designed to pass all tidal components of species m without change of amplitude or phase and to eliminate all other species. The 'imaginary' member has the same filter characteristic but imposes a $\frac{1}{2}\pi$ phase shift. We may call the result of convoluting $\xi(t)$ with this pair of filters $\chi_m(t)$, where

$$\chi_m(t) = \xi_m(t) + \mathrm{i}\xi_m^*(t).$$

Details of the filters used here (members of a general family generated by a computer program) are given in appendix C.

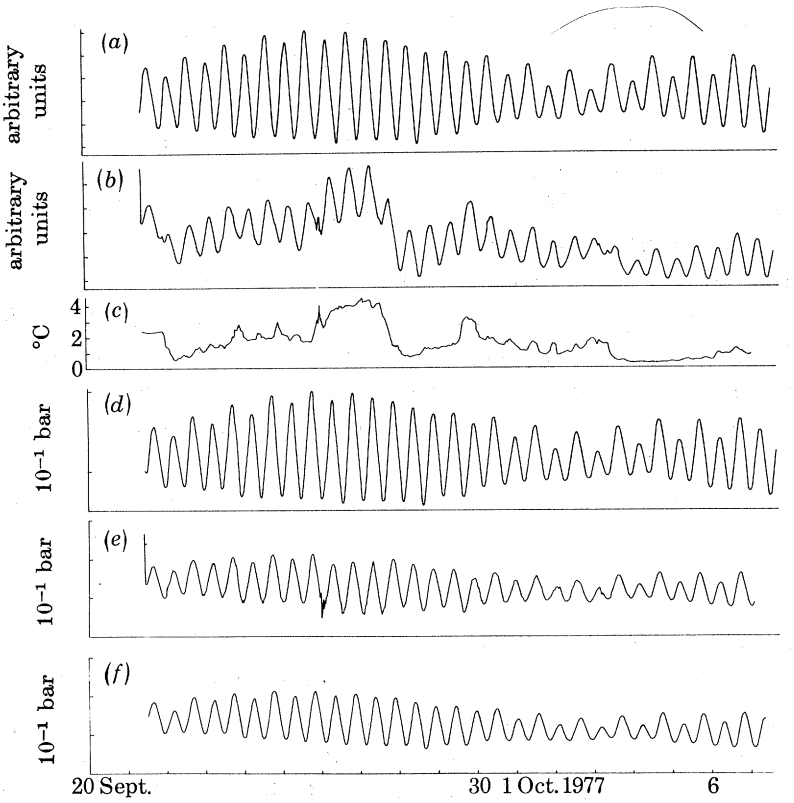

FIGURE 4. Raw frequency data from (*a*) quartz crystal sensor and (*b*) strain gauge sensor on capsule at position R2, in temperature variations shown in (*c*). (*d*), (*e*) Pressure signals from the quartz crystal and strain gauge sensors after calibration involving a static temperature correction. (*f*) Pressure signal from strain gauge sensor after dynamic temperature correction.

Before correlating a given tidal signal $\zeta(t)$ with $\chi_m(t)$ we first removed instrumental drift from the pressure record in the form of a low-order polynomial in t, determined by least-squares. The part of the drift-free signal $\zeta(t)$ which is coherent with the species components of the reference tide was then evaluated by inversion of the matrix of cross-correlations between the variables (according to the standard 'least squares' principle) to express the signal optimally in the form

$$\zeta(t) = \sum_{m=1}^{3} [a_{m0}\,\xi_m(t) + b_{m0}\,\xi_m^*(t) + a_{m1}\,\xi_m(t-\tau) + b_{m1}\,\xi_m^*(t-\tau)] + r(t) \qquad (1)$$

where a_{mn}, b_{mn} are constants, τ is an arbitrary time-lag of 2 days (Munk & Cartwright 1966) and $r(t)$ is the uncorrelated part of $\zeta(t)$, consisting principally of low frequency variations and

general 'noise'. When the constants in (1) had been evaluated, both $\zeta(t)$ and $r(t)$ were spectrally analysed to give their partial variances in frequency bands centred on and covering the three species, as a means of estimating noise:signal ratios. (The frequency bandwidths for all species were invariably 9 cycles per month or 0.33 cycle per day (c/d)).

The precise form of the scheme (1) was chosen, as a result of several tests employing greater numbers of time-lags and leads, as being a good compromise between simplicity and 'wiggliness' of the corresponding admittance function between ζ and χ_m (a dilemma explored by Zetler & Munk 1975). It absorbs as much of the tidal variation in $\zeta(t)$ as can be justified from records of order 28 days' duration. More arguable than the choice of the number of arbitrary terms is the choice of the reference tide $\tilde{\zeta}(t)$ itself. One has the option of taking $\tilde{\zeta}(t)$ to be either the gravitational potential, or a tidal synthesis based on the potential but incorporating local peculiarities in the admittance, solar radiational components and other terms, known to exist at local shore stations. Walter Munk and his associates tend to use the potential directly, allowing rather more terms in (1) to model the full admittance function. Zetler & Munk (1975) make a concession to local peculiarities by effectively replacing t in (1) by $(t-T_m)$, where T_m is the 'age' of the local tide of species m. On the other hand, comparative tests of methods of analysis of a 30-day record from north Shetland described in Unesco (1975) showed distinct improvement in residual variances when a tidal synthesis for Lerwick was taken as reference tide.

We have chosen to take tidal syntheses from a few well-exposed coastal ports as reference tides for our pelagic records. Our reasons are their proximity, the virtual absence of amphidromic points within our area, the peculiar shape of the local diurnal admittances and the presence of a marked semi-diurnal radiational anomaly at all stations where it can be resolved, including islands. The last two characteristics would be hard to model directly from the gravitational potential with a few arbitrary terms as in (1). The chosen scheme gives consistent results and low noise residuals. In the next sub-section we describe the characteristics of our reference tides.

(*b*) *The reference tides*

Details of the ports used for tidal reference are listed in table 1. They all have records of sea level, taken at hourly intervals for more than five years, from which their tidal constants have been derived. After careful checks to eliminate errors, all these records were subjected to 'response' analysis in terms of the lagged gravitational and radiational potential functions listed at the foot of the table. These variables have been found adequate to delineate the shape of the principal admittances across their species bands and to resolve the lesser effects such as those resulting from solar radiation and spherical harmonics of third degree (Cartwright 1968, 1975, 1976*b*).

The only nonlinear term included in the analysis is that denoted by I^{2+2-2}, a semi-diurnal third-order interaction well known to be generated by friction in areas where the tidal range is large. The coefficient of this term had significant size only at St Mary's, owing to the proximity of the English Channel and the Bristol Channel. 'Overtides' such as the quarter-diurnal I^{2+2} were also present in some records but are irrelevant in this work because if included in the synthesis $\tilde{\zeta}(t)$ they are removed by the filtering procedures. The frictional I^{2+2-2} term was however excluded from the formulation of $\tilde{\zeta}(t)$ because it is demonstrably absent from the open sea.

Apart from the above, reference tides $\tilde{\zeta}(t)$ were generated from the 'response weights' derived from the 5–9 year analyses of the chosen places according to a formalism of type

$$\tilde{\zeta}(t) = \mathrm{Re}\,\Sigma w^*_{ks}\, V^m_n(t-s\tau) \qquad (2)$$

discussed in Munk & Cartwright (1966) and other papers, where $V^m_n(t)$ are precisely computed

coefficients of the spherical harmonics of the tide-generating potential. (It is perhaps worth reminding some readers that formalism (2) embodies the full gamut of time-harmonics, nodal modulations, etc., familiar to users of the 'harmonic method'.)

TABLE 1. STATIONS USED FOR REFERENCE TIDES

name	position	no. of years	period analysed	pelagic stations using reference
Lerwick (Shetland)	60° 09′ N 1° 09′ W	6	1959–64	S5–9 (BA, FL)
Stornoway (Hebrides)	58° 12′ N 6° 23′ W	6.5	1959–61 1968–71	S1–4, S13, S14, D0, R3, F5, F6 (SK)
Malin Head (Eire)	55° 23′ N 7° 24′ W	6	1960–64 1966–68	Not used
St Mary's (Scilly I.)	49° 55′ N 6° 20′ W	6	1968–74	C1–8, D1, D5, D6 (PM, BO)
Brest (France)	48° 23′ N 4° 30′ W	6	1921(3)36	C1, D1, D1′
Lagos (Portugal)	37° 06′ N 8° 40′ W	9	1966–74	M1, M2, D2, D4
Terceira (Azores)	38° 40′ N 27° 14′ W	5	1957–62	M3, M4, D3, D10
Reykjavik (Iceland)	64° 09′ N 21° 56′ W	9	1966–74	R1, R2, D7–9

Potential variables used: $C_2^1(0, \pm 2, \pm 4)$, C_3^1, R_1^1, R_2^1; $C_2^2(0, \pm 2, \pm 4)$, C_3^2, R_2^2, $C_3^3(0, \pm 2)$.

The admittances of the reference tides to the principal terms of species 1 and 2 in the gravitational potential are shown in figure 5 for all reference stations used for analysing both the shelf-edge and the oceanic sites. The curves describe the variation with frequency of the real and imaginary parts of

$$\ln Z = \ln R + \mathrm{i}\phi,$$

where Z is the admittance function in the normalization of Munk & Cartwright (1966), $R = |Z|$ is the magnification factor and ϕ is the phase lead with respect to Greenwich transit. Thus, harmonic amplitudes are given by R multiplied by the corresponding harmonic amplitude in the potential as detailed by Cartwright & Edden (1973), and Greenwich phase lags are given by

$$G = m\pi - \phi.$$

The advantage of plotting $\ln Z$ is that local magnifications and phase lags uniformly affecting the whole frequency band merely raise or lower the curves without altering their shape.

One sees from figure 5 that the admittances for any species are closely related in shape throughout the region, no doubt reflecting the frequency response of the ocean as a whole. Cartwright (1968) showed some similar results including ports in the North Sea, but based on shorter data series. For species 2, magnifications are of order $e^{1.5}$ or 4.5 times greater than for species 1, as is well known to occur in the Atlantic Ocean, and the phase leads all decrease uniformly with frequency in accordance with the typical local 'age' of about 36 h. In so far as the semi-diurnal tides of the North Atlantic may be said to resonate, their admittance shows remarkably little of the structure normally associated with a resonance peak across the given bandwidth. One must assume that dissipation, or the combined effects of several close normal modes, broadens the resonance peak over a band wider than 0.2 c/d. Platzman (1975) computed normal modes with periods 11.35, 12.17, 12.79 and 13.77 h in his numerical model of the combined Atlantic and Indian Oceans; these periods are all within or just outside the band represented in figure 5.

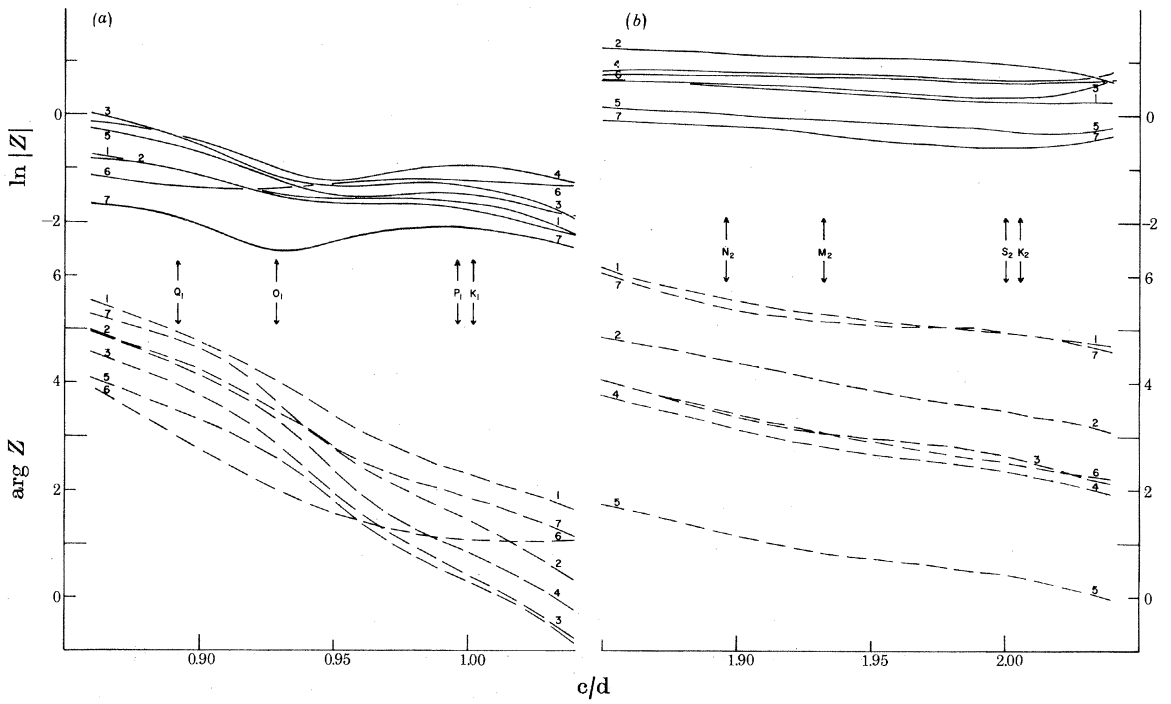

FIGURE 5. Real (——) and imaginary (– – –) parts of ln Z, where Z is admittance to the gravitational potential for (*a*) diurnal tides and (*b*) semi-diurnal tides, for the following reference stations: (1) Lagos; (2) Scilly Isles; (3) Malin Head; (4) Stornoway; (5) Lerwick; (6) Reykjavik; (7) Azores. ↓, Frequencies of the principal harmonic constituents.

The diurnal admittance curves for the western stations, numbered 1–5 in figure 5, are again very similar in shape, with a slight dip in the magnification at about 0.95 c/d and a pronounced age of order 5 days. The enhanced phase gradient at the frequency of the dip in magnification suggests an anti-resonance to the principal (2nd degree) diurnal generating potential. Cartwright (1975) showed that the 3rd degree potential which is chiefly manifest in a small harmonic line at precisely 1 cycle per lunar day (0.966 c/d), is considerably enhanced at these and other northwest European ports, so that the line has locally greater amplitude than the neighbouring lines from the 2nd degree potential. This fact showed that the anti-resonance evident in figure 5 and the apparent resonance of the 3rd degree potential are dependent on the spatial matching of the generating function and the wave form of the normal oceanic modes near 1 c/d. The dip in magnification is most pronounced at the Azores (no. 7 in figure 5), though at a slightly lower frequency, and is also distinct as far south as Ascension Island and Simons Bay, South Africa (Cartwright 1971).

The least conformable of the diurnal admittances is that for Reykjavik (no. 6). Here the magnification is nearly flat and the age as measured by the phase gradient much reduced. This marks the beginning of a trend towards the conditions in the north western Atlantic where the age of the diurnal tides is practically zero; probably due in part to near-resonant co-oscillation of the Greenland Sea (Huthnance 1980*a*).

(c) *Radiational tides*

The only radiational tides of any importance were as usual, in species 2, with S_2 (two cycles per solar day) as the harmonic constituent most affected. Table 2 lists the amplitudes and phase lags of the gravitational (H_g, G_g) and radiational (H_r, G_r) contributions to S_2 resulting from response analysis of each reference station, and also the amplitude ratios and phase differences of these components. The ratios, of order 0.15, and phase differences, of order 120°, are similar to those of previous evaluations (Cartwright 1968; Zetler 1971), and confirm an effect, somehow related to the solar tide in surface atmospheric pressure, as being present over the whole ocean area considered.

TABLE 2. COMPONENTS OF S_2

station	H_g/mm	G_g/deg	H_r/mm	G_r/deg	H_r/H_g	(G_r-G_g)/deg
Lerwick	22	336	4	88	0.18	112
Stornoway	57	224	8	347	0.15	123
Malin Head	40	208	4	293	0.10	85
St Mary's	76	161	11	305	0.14	144
Lagos	37	76	4	193	0.11	117
Terceira	16	75	2	165	0.13	90
Reykjavik	55	215	6	347	0.11	132

The most noticeable effect of the radiational anomaly is that the phase lag of the total S_2 constituent is a few degrees greater than its higher frequency neighbour K_2, the reverse of the general trend of phases across the semi-diurnal band. Because of our method of reference, such an anomaly is evident in the harmonic constituents S_2 and K_2 from all our pelagic records (appendix A).

(d) *Analysis of pelagic records*

Most pelagic pressure records were assigned a reference tide from the nearest of the places in table 1, but this was less appropriate for the western ocean stations and for some of the shelf stations near Ireland. In cases of doubt we analysed in terms of two alternative references and chose the one giving the smaller variance in $r(t)$. By that process, we found that, for example, Malin Head always gave larger residual variances than Stornoway or St Mary's and was therefore not used to produce any of the final results. This may be because of the frequent silting of the gauge at Malin Head noted in Cartwright (1968), although the very bad period of silting in early 1960 was omitted from the present analysis.

After the constants a_{mn}, b_{mn} appropriate to (1) had been evaluated, the relative admittance or 'transfer function' between reference tide and pelagic record,

$$Z_m(f) = a_{m0} + \mathrm{i}b_{m0} + (a_{m1} + \mathrm{i}b_{m1}) \exp(-2\pi \mathrm{i} f\tau) \tag{3}$$

was computed at frequencies f of interest, and the major harmonic constants H, G evaluated from

$$H = |Z_m(f)|\tilde{H},$$
$$G = \tilde{G} - \arg[Z_m(f)], \tag{4}$$

where $\tilde{H}$, $\tilde{G}$ are the constants of the reference tide.

Relative standard errors σ_m were then estimated for each species according to the empirical formula

$$\sigma_m^2 = \frac{1}{2}\left|\frac{v_r}{v_s - v_r}\right|\frac{27.3}{D}, \tag{5}$$

where v_s and v_r are the variances of (band filtered) signal and residual respectively, and D is the duration of the record in days. (This formula can be roughly justified for a uniform spectral distribution of noise, and in practice appears to give realistic values.)

All results from pelagic stations are tabulated in appendix A. Island stations, the records of which were taken by I.O.S., were analysed by a somewhat more elaborate but related method, in keeping with their longer time span, usually of the order of several months. Their harmonic constants are listed in appendix B, together with some results from our analysis of data supplied by other authorities, and some other relevant constants taken from published sources.

6. Shelf-edge tides

(*a*) *Tidal currents*

We accompanied most of the shelf-edge pressure recordings with recordings of similar duration of the current about 25 m above the bottom to determine the pressure gradients normal to as well as along the line of stations and the power flux on to the shelf. Pressure gradients and power flux are strictly expressed in terms of the depth-mean current, so one needs some assurance that the tidal current at 25 m is representative of the whole water column, typically 150 m deep, or to have some simple conversion factor.

We therefore measured vertical profiles of the currents wherever convenient, principally south of St Kilda and near Rockall, Foula and Unst. This was done with the ship at anchor, lowering or raising a Kelvin and Hughes 'direct reading current meter' between surface and bottom with a pause for a reading of speed and direction at 10 m intervals. One such profile occupied typically 15 min, and was repeated at half-hourly intervals for 2–5 lunar days. Such operations were possible only in fairly calm weather, but we obtained good readings with local winds of velocities up to 12 m s^{-1}.

Figure 6 shows the results from our longest and best current profile, recorded at 57° 21′ N, 8° 35′ W, 50 km due south of Hirta (St Kilda group), for a continuous period of 125 h, 8–13 July 1968. The bottom was flat and sandy with a mean depth of 147 m. The region is known for the prominence of its diurnal currents (Cartwright 1969), so it was possible to obtain reliable results for tides of both species 1 and 2 from only a few days' record, unlike at other similar stations. The 250 pairs of north and west current components recorded at each depth were correlated with the simultaneous tidal synthesis for Stornoway, after the manner described in § 5 (*d*) but without employing time lags τ in (1) and (3) because the shortness of the records would not justify such resolution. The real and imaginary parts of the constant admittance Z_m so evaluated both for species $m = 1, 2$ and for directional components are plotted against depth in figure 6.

The units of Z_m are m s^{-1} per metre of tide at Stornoway, that is s^{-1}. The largest values of Z_1 are seen to be about five times the largest values of Z_2, because of the larger diurnal inequality in the currents in the St Kilda region. With harmonic constants at Stornoway (0.13 m, 134°) for K_1 and (1.36 m, 198°) for M_2, typical current amplitudes are 0.15 m s^{-1} for K_1 and 0.30 m s^{-1} for M_2. The ellipses for the depth-mean currents of both species are shown in the lower panel in admittance units. They are in line with those recorded with better harmonic resolution at other stations in the area, depicted in Cartwright (1969) where other statistics are listed.

It is surprising that the species 2 current profiles show considerable vertical shear while the species 1 profiles are almost uniform. The shear in the upper layers for species 2 is evidently

related to the density profile recorded at the time and shown top right of figure 6, but calculation of internal shear stresses by integration of the momentum equations from the surface downward after the manner of Bowden & Fairbairn (1952) gave erratic results, not clearly related to the vertical shear itself. One must assume that the vertical current structure is a reflection of internal motions in the local deep ocean, transmitted over the shelf by horizontal shear stresses. In the lower regions, where the density is nearly uniform, the profiles show a turbulent boundary layer

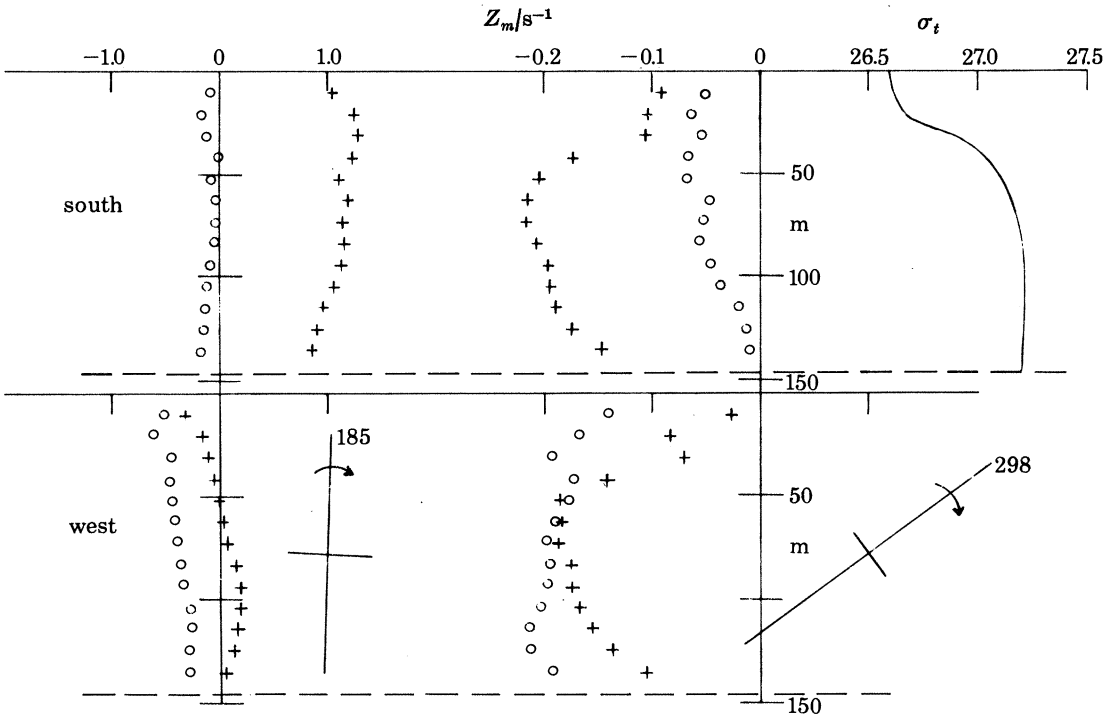

FIGURE 6. Results of analysis of current profiles for a 125 h period at 57° 21′ N, 8° 35′ W, 8–13 July 1968. ---, Bottom (147 m). ——, Top right, shows density profile in units of σ_t. + (real) and o (imaginary), admittances of south and west components of current with respect to tidal elevation at Stornoway; admittances of diurnal tides on the left, semi-diurnal tides on the right. Dimensions and orientation of tidal ellipses of depth-mean current are shown in the lower half (north vertically upwards), where the number gives the phase lag on Stornoway when current is along the major axis, and the arrow denotes sense of rotation.

associated with friction on the bottom. The structure will change as the summer thermocline (as shown) is eroded by storm waves. By taking the vertical structure as typical of summer conditions in this shelf region (all current records being subsequently taken in the summer), the relation between the depth-mean current $\bar{\boldsymbol{v}}$ and the current recorded 25 m above the bottom, $\boldsymbol{v}_{25}$, could be well enough expressed by the relations

$$\bar{\boldsymbol{v}} \approx 1.16\,\boldsymbol{v}_{25} \quad \text{(species 1)},$$

$$\bar{\boldsymbol{v}} \approx 0.92\,\boldsymbol{v}_{25} \quad \text{(species 2)}.$$

These relations were used in subsequent calculations that involved direct measurements of current, except where the depth-mean current was obtained locally from other profile measurements.

(*b*) *Pressure gradients*

Wherever we recorded currents and pressure together, we computed pressure gradients from the dynamic equations, as follows. Taking local cartesian coordinates x, y, z, with x north, y west and z vertically upwards, and corresponding components of depth-mean current $\bar{u}$, $\bar{v}$, $\bar{w}$ at depth h and time t, we have (cf. Hendershott 1972)

$$\left.\begin{aligned}\frac{\partial\zeta}{\partial x} &= -g^{-1}\left(\frac{\partial\bar{u}}{\partial t}+2\Omega\sin\theta\,\bar{v}+\frac{F_x}{h}\right)+\frac{\partial}{\partial x}(0.69\zeta'+\zeta''),\\ \frac{\partial\zeta}{\partial y} &= -g^{-1}\left(\frac{\partial\bar{v}}{\partial t}-2\Omega\sin\theta\,\bar{u}+\frac{F_y}{h}\right)+\frac{\partial}{\partial y}(0.69\zeta'+\zeta''),\end{aligned}\right\} \tag{6}$$

where ζ is the tidal elevation relative to the sea bed, ζ' is the tide-generating potential divided by gravitational acceleration, g, Ω is the Earth's angular velocity, θ is latitude, and F_x, F_y are components of frictional bottom stress divided by water density. The factor 0.69 in (6) is the well-known combination of Love numbers $(1+k_2-h_2)$ which allows for the direct elastic yielding of the Earth's crust to the tidal forces and its potential (the 'body-tide'), while ζ'' represents the yielding and potential resulting from the ocean tide (the 'loading-tide').

The loading-tide is generally smaller than the body-tide, and since it requires calculation of a large number of spherical harmonics of the ocean tide with their associated Love numbers (Hendershott 1972), and both terms are much smaller than the leading terms in (6), we omitted ζ'' from the calculation of pressure gradients.

The terms involving bottom stress are also fairly small, with depths of order 100 m and speeds of order 0.1 m s^{-1}, so they may be well enough approximated by the linearized forms

$$(F_x, F_y) = 0.0025\bar{c}(\bar{u}, \bar{v}), \tag{7}$$

where $\bar{c}$ is the r.m.s. speed of the current, typically 0.2 m s^{-1}, and the factor 0.0025 is the coefficient usually applied to quadratic bottom stress.

With the above approximations, we assumed a time dependence $\exp(-i\omega t)$ in all linear variables, and used the measured harmonic constituents of u and v and the known amplitudes of ζ' (Cartwright & Edden 1973) to derive from (6) the harmonic constituents of the derivatives of ζ. As first shown by Proudman & Doodson (1924), these are most usefully applied to the construction of cotidal maps by converting them to the spatial derivatives of H and G, the amplitude and Greenwich phase lag of the harmonic constituent concerned. Thus, in terms of complex quantities, starred for the conjugate,

$$\left.\begin{aligned} H = |\zeta|,\quad \frac{\partial H}{\partial x} &= H^{-1}\,\mathrm{Re}\left(\zeta\frac{\partial\zeta^*}{\partial x}\right),\quad \frac{\partial G}{\partial x} = H^{-2}\,\mathrm{Im}\left(\zeta\frac{\partial\zeta^*}{\partial x}\right),\\ \frac{\partial H}{\partial y} &= H^{-1}\,\mathrm{Re}\left(\zeta\frac{\partial\zeta^*}{\partial y}\right),\quad \frac{\partial G}{\partial y} = H^{-2}\,\mathrm{Im}\left(\zeta\frac{\partial\zeta^*}{\partial y}\right).\end{aligned}\right\} \tag{8}$$

The vector gradients of H and G derived from (6) and (8) for the M_2 constituent are represented at every current-meter station in figure 7*a*. Gradients of H ($\rightarrow$) mostly conform to the general property of Kelvin waves, that amplitudes increase towards the nearest coast, whether this be the mainland or a sizeable group of islands such as the outer Hebrides or Shetland. Exceptions are seen west of Norway and northwest of the Faeroes, where the gradient vector points away from a known amphidrome in each case. (Currents at the deep (375 m) station S11 off Norway were recorded by a moored string of three current meters.)

PHILOSOPHICAL TRANSACTIONS OF THE ROYAL SOCIETY A MATHEMATICAL, PHYSICAL & ENGINEERING SCIENCES

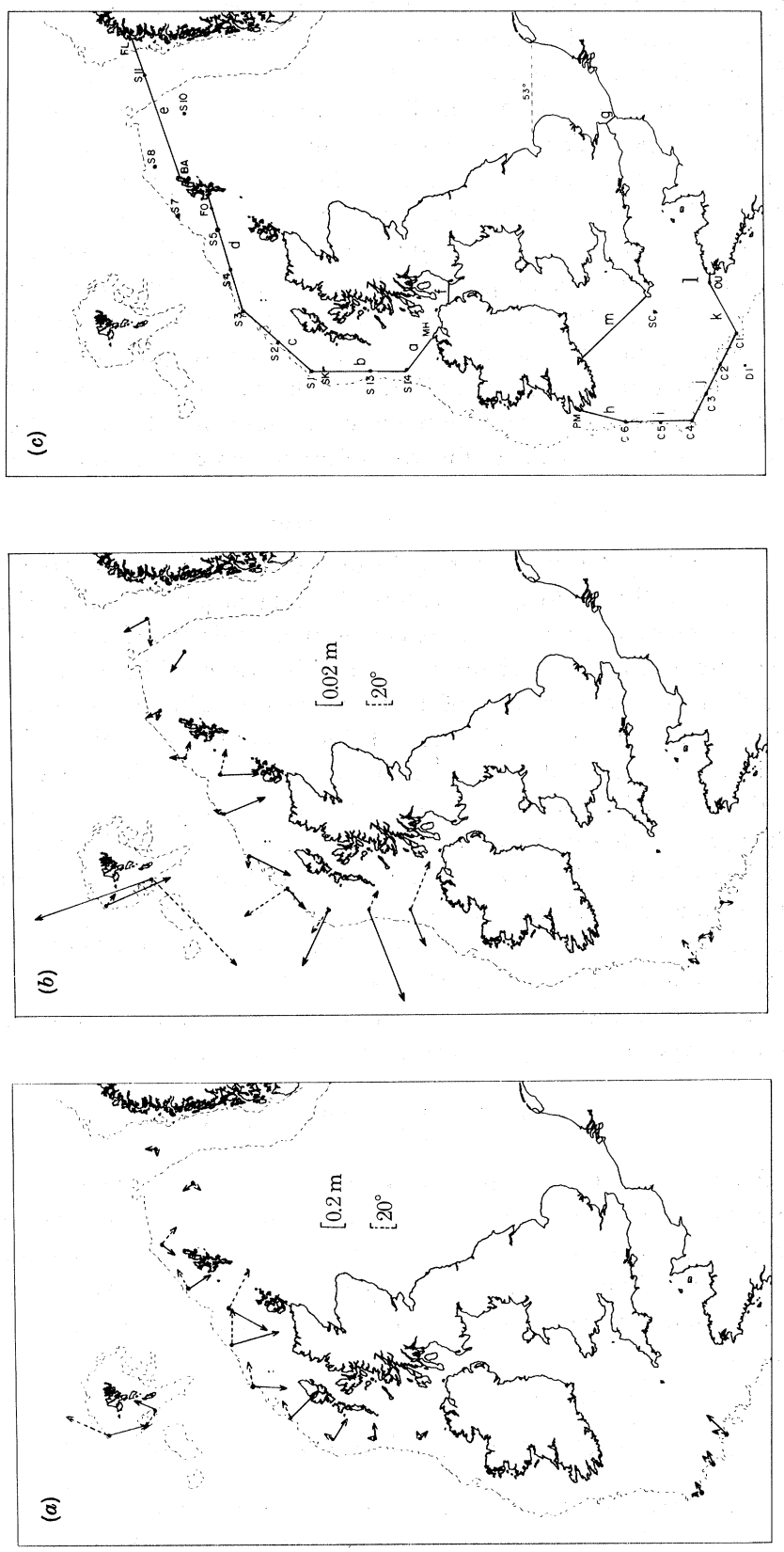

FIGURE 7. Spatial gradients, amplitude H (→) and phase lag G (----→), deduced from current and pressure records near the shelf-edge: (*a*) M_2; (*b*) K_1. (*c*) Boundaries used for calculations of tidal power flux (cf. table 2); station positions are also shown.

It is interesting that the more southerly of the Faeroes stations shows increase of amplitude towards the islands, which is apparently contradicted by the well-known low semi-diurnal amplitudes at Thorshavn (appendix B). However, the landward increase across the western Faeroe shelf is confirmed by the M_2 amplitudes at station F5 (0.56 m) and at Sørvagur (0.67 m), a western Faeroese port. The nearly amphidromic regime at Thorshavn (0.10 m) must be confined to the eastern Faeroe shelf. The sharp difference in amplitude across the narrow north–south chain of islands accounts for the notoriously strong currents which flow through the gaps.

Gradients of phase lag G (----➤) in figure 7*a* tend to follow the shelf contour in the expected direction where backed by land, particularly in the northwestern area, but where an open sea presents itself, as in the Celtic Sea in the southwest and the North Sea in the north of the map, the vectors tend to point into the sea, in accordance with wave propagation into such areas. The slight westerly progression of phase indicated at the two stations close to Norway is again in accordance with the anti-clockwise amphidrome off southwest Norway which has appeared in cotidal maps of the North Sea since the work of Proudman & Doodson (1924).

(*c*) *Power flux*

Another valuable quantity which may be derived from the combination of tidal elevations and currents round the shelf-edge is the flux of energy or power into the shelf sea as a whole. In so far as the energy which enters the sea across its oceanic boundaries, and a slight increment from direct interaction with tidal forces, are entirely dissipated by friction on the sea bed, it is relevant to the long-term energetics of the Earth–Moon orbital system, with many geophysical implications. Direct measurement is especially important because estimates of the global power loss from tidal friction in shallow seas based on more or less rudimentary hydrographic information (Miller 1966) fall considerably short of those deduced from astronomical observations (Lambeck 1977). While the loss in the well-documented seas round Britain is less likely to be as badly estimated as that in the Bering Sea used to be before the work of Sündermann (1977), and there are many other shallow seas which are more in need of proper measurement, nevertheless this was the first opportunity to make a direct estimate of the loss from a coordinated set of measurements surrounding an important area of dissipation.

As pointed out by Garrett (1975), the energy equation for tides in a partially enclosed sea may be written two ways which are sometimes confused. One form is

$$\int gh\,\langle\zeta u_{\mathrm{n}}\rangle\,\mathrm{d}s = \int \langle \boldsymbol{u}\cdot\boldsymbol{F}\rangle\,\mathrm{d}A - \int gh\,\langle \boldsymbol{u}\cdot\nabla\zeta_{\mathrm{e}}\rangle\,\mathrm{d}A, \tag{9}$$

where the first integral is taken along an arbitrary contour which defines the boundary between the sea and the external ocean, u_{n} is the inward-pointing normal component of depth-mean velocity, and $\langle\ \rangle$ denotes a mean value over a tidal cycle. The second and third integrals are taken over the area of the sea and represent the rate of work per unit mass against respectively the bottom friction and the tide-raising stress, where $\boldsymbol{u}$ denotes $(\bar{u}, \bar{v})$ and $\zeta_{\mathrm{e}} = 0.69\zeta'$ is the 'equilibrium tide'.

The second form of energy equation is

$$\int gh\,\langle(\zeta-\zeta_{\mathrm{e}})\,u_{\mathrm{n}}\rangle\,\mathrm{d}s = \int \langle \boldsymbol{u}\cdot\boldsymbol{F}\rangle\,\mathrm{d}A - \int g\,\langle\zeta_{\mathrm{e}}\,\partial\zeta/\partial t\rangle\,\mathrm{d}A. \tag{10}$$

Choice between these two forms depends partly on one's preference for the physical meaning of the alternative left side integrals and partly on which of the alternative final integrals is easiest

to compute with the given data. Robinson (1979), in his detailed study of the tidal energetics of the Irish and Celtic Seas, called the quantities on the left sides of (9) and (10) the 'apparent' and 'corrected' energy flux respectively, although he also included a small correction for the Earth's loading tide. We took the view that, since a realistic array of $\boldsymbol{u}$ vectors over the sea area is in any case required to evaluate the frictional dissipation, we may as well use it for the third integral of (9), whose left side also arises more directly from the measured data. We therefore worked in terms of (9) although we also evaluated the integral on the left of (10), and found like Robinson (1979) that the difference is very small. The difference in formalism may well be critical in discussing the diurnal tides where ζ and ζ_e have more comparable magnitudes.

Figure 7*c* shows the boundaries and areas over which we evaluated the integrals in (9) and on the left of (10). The boundaries are obviously chosen to pass through our pressure and current stations and to terminate at points of land where reliable tidal constants were obtainable from our own or other records (appendix B). The principal current-meter stations on the boundary are as shown in figures 7*a*, *b*, but to obtain better definition of currents near the land terminal points we took additional short current-profile records near the landward ends of sections *a*, *d* and *e*. A current-meter mooring at station C6, south of Valentia, proved to have instrumental defects, but some information was available from a British Admiralty current station at (50° 37′ N, 10° 16′ W); in fact power flux across *h* and *i* is not critical.

We should have liked more reliable data in the region of section *k* where the power flux is quite large, but proliferation of fishing trawlers and submarines makes this area hazardous for moored instruments. We made use of some current records by Cartwright & Woods (1963) near C1, and some data at stations near Ouessant published by the 'Service Hydrographique et Oceanographique de la Marine' (1968). The notorious tidal races in section *l* between Ouessant and the French mainland gave negligible power flux because they are largely in quadrature with the tidal elevation.

In addition to computing power fluxes across the outer boundary, we also computed power fluxes across the narrow sections *f* (North Channel) and *g* (Dover Strait), to separate the distinct dissipating regions of the North Sea and the seas to the south and southwest of Britain. For data across *g* we used the line of current stations by Cartwright (1961) and tidal elevations at Dover and Sangatte. For the deeper section *f*, we used current data from three moorings, each bearing three current meters recording for over a month in 1971 spanning the channel at about 55° N (Howarth, M. J. & Loch, S. G. 1973, U.K. Inst. Oceanogr. Sci. (I.C.O.T.) Data rep. no. 3 – unpublished) and tidal elevation data along the same latitude interpolated from stations on the Scottish and Irish coasts in that region.

The results for fluxes across the two oceanic boundaries and channels *f* and *g* are detailed in table 3. The differences between integrals (9) and (10) vary slightly, but reduce to a negligible amount between the totals for the northern boundary because of the considerable change in phase of ζ along the contour while the phase of ζ_e varies very little. The difference between (9) and (10) is more marked along the southern boundary where the phase of ζ is almost constant. It is interesting to compare these figures with those obtained by Flather (1976) from a computer model of the whole shelf sea driven by our boundary data for M_2 tidal elevations but not using our boundary currents. Flather's energy flux was largely determined by arbitrary radiation conditions along the boundary, adjusted to give nearly correct coastal elevations, with dissipation in the interior as determined by a standard quadratic frictional term. The northern boundary of Flather's figure 9 (adding our value for 'a' to effect a closure to the Irish coast)

PHILOSOPHICAL TRANSACTIONS OF THE ROYAL SOCIETY A MATHEMATICAL, PHYSICAL & ENGINEERING SCIENCES

gives 48.1 GW compared with our 60.0 GW. This is certainly too small, and is exacerbated by a negative flux of −5 GW across a section corresponding roughly to our section *e*. On the other hand, Flather obtains 180 GW for his Celtic Sea boundary which is again somewhat lower than our value of 190 GW, but is in very reasonable agreement in terms of proportions.

Our total figures for the total M_2 dissipation in these shelf seas, 250 GW for (9) and 243 GW for (10) should be definitive. They are distinctly greater than the earlier estimates of type (9), namely 120 GW (Jeffreys 1920), 143 GW (Heiskanen 1921) and 163 GW (Miller 1966), where the first and second figures are reduced from their original spring tide rate to mean rate as listed in Miller's table. However, the effect of this increase on Miller's (1966) global estimate of $1.7/10^3$ GW is marginal and more than compensated for by the reduction in the loss in the Bering Sea from 240 (Miller 1966) to 29 GW (Sündermann 1977).

TABLE 3. POWER FLUXES ACROSS BOUNDARIES/GW

	northern boundary (9)	northern boundary (10)		southern boundary (9)	southern boundary (10)
a	4.4	4.5	*h*	30.6	31.3
b	17.2	17.6	*i*	37.3	38.2
c	14.1	14.6	*j*	82.9	77.2
d	12.1	12.1	*k*	39.2	36.3
e	12.2	11.4	*l*	0.0	0.0
totals	60.0	60.1	totals	190.0	183.0
across channels (positive towards north)					
f	0.1	−0.4			
g	16.7	16.2			
m	44.9	45.1†			

† From Robinson (1979).

Our figure for the important power flux through channel *g*, the Dover Strait, does not appear to have been estimated before from direct measurements, but Flather (1976) quotes a value of 16.1 GW from his computed model, which is very close to our value. Our estimates for the North Channel, *f*, are very small, as are those of Taylor (1919) and Robinson (1979), but Robinson obtained a distinctly greater northward flux of 2 GW. Our result, based on nine current-meter records, is probably more reliable than Robinson's based on two, but the result for practical purposes is zero.

Taking Robinson's (1979) results for the flux across a section *m* between St Ives (Cornwall) and Cobh (Eire), reproduced in table 3, as definitive, we deduce the following figures for the dissipation in the English Channel and southern part of the Celtic Sea.

Integrals (9): $190.0 - 44.9 - 16.7 = 128.4$ GW;

integrals (10): $183.0 - 45.1 - 16.2 = 121.7$ GW.

These are again more than twice the estimate of 50 GW by Miller (1966) and his predecessors for the English Channel alone, and significantly greater than the dissipation of 98.5 GW derived by Flather (1976) for a similar area which includes a slightly larger portion of the Celtic Sea. We computed the integrals to the right of (9) only for the area north of the channel boundaries *f* and *g* bounded by the external contour *a*–*e*, that is for the North Sea and the seas to the north and west of Scotland. This area dissipates less than half the energy lost in the remainder of the shelf sea, but we have more comprehensive data for the input along the northern shelf boundary, and the chosen area provides a good enough test of what can be done with the interior current

data. For the latter, we used the currents represented in one-third-degree rectangles over the whole shelf sea in the D.H.I. (1963) Atlas. These are based on interpolation between measured currents, of generally greater density where the sea is shallow and the currents strong. They are therefore likely to be more realistic than currents taken from a computer model of the sea. The complete array of speeds and directions represented in hourly steps from 6 h before to 6 h after Greenwich transit were carefully digitized, and the time sequence at each grid point harmonically analysed into complex current amplitudes $(r\bar{u}, r\bar{v})$ for M_2, where r is an arbitrary factor, taken as 1.5, which allows for the fact that the given figures represent mean spring-tide conditions near the sea surface. (In most of the North Sea, the amplitude ratio $(M_2+S_2:M_2)$ is about 1.3; the factor 1.5/1.3 reasonably accounts for known surface/mean ratios, as in Cartwright (1961).)

Table 4. Internal power loss in North and Scottish seas/GW

	against friction	against Moon	total	from Flather (1976)
north of 53°	26.1	1.4	27.5	32.1
south of 53°	12.3	−0.1	12.2	16.7
total	38.4	1.3	39.7	48.8

The mean rate of working against the frictional bottom stress for each grid area dA was calculated by the usual quadratic friction law as

$$\langle \boldsymbol{F}\cdot\boldsymbol{u}\rangle\, dA = 0.0025\,\langle|\bar{u}^2+\bar{v}^2|^{\frac{3}{2}}\rangle\, dA, \tag{11}$$

where the average over a tidal cycle was computed by numerical integration. The second integral in (9), describing the work done against the horizontal tidal stress, was also evaluated for each area dA by a simple function of $\bar{u}$, $\bar{v}$, latitude and longitude. Robinson (1979) also added the work done against the loading Earth-tide in the Irish and Celtic Seas. We have omitted this because it is very small compared with errors in say (11), and particularly so in the North Sea, where the amplitude of the loading tide is itself very small on account of distance from the principal effective loading area of the North Atlantic west of the Celtic Sea, and occasional antiphase of the Atlantic loading and the local North Sea loading (Baker 1979). Robinson's correction for the loading tide in the Celtic Sea was less than 0.3 GW, in an area of maximum loading, some four times greater than the largest values in the North Sea.

The results of these calculations are presented in table 4, with a division between the small sea-area south of 53° N latitude with generally strong currents and the much larger areas to the north where the currents are strong in places but are mostly weaker. The contribution from the second integral of (9) (second column) is quite small, as usual, because of the rapid changes of the phase of $(\bar{u}, \bar{v})$ over the area with little change of the phase of $\nabla\zeta_e$. The third column is simply the sum of the preceding columns and is compared with corresponding figures (without the work against the Moon) from Flather's (1976) model. Flather's computations used exactly the same formula as (11) over a similarly sized grid but with depth-mean currents $(\bar{u}, \bar{v})$ derived from the finite-difference solution of the dynamical equations. They are fairly similar to ours in magnitude, but a little greater. However, both our total of 40 GW and Flather's of 49 GW are conspicuously less than the total input through the boundaries *a*–*g* from table 3, namely 77 GW.

Similar discrepancies between external power input and internal loss from bottom friction were found by Robinson (1979) in the seas between sections *f* and *m*. Indeed, the only plausible balance between the two rates of working was that found by the pioneer of this subject, Taylor

(1919), in application to the Irish Sea. However, Taylor used very sparse data for the interior currents, and his estimate of the frictional loss after allowing for his use of spring-rates is about twice the value of Robinson (1979) for the same area based on extensive recent current data. Although the dependence of (11) on the cube of the current speed makes it sensitive to small errors of estimation, it is hardly possible to make up the gap in the power budget by adding fine-scale current data for coastal inlets and passages between islands, or by adjusting the coefficient. We must conclude from these results and from Flather's and Robinson's work that there is another sink of dissipation within the shelf sea area besides that caused by bottom shear. Investigation of such a sink is outside the scope of this paper, but likely areas are horizontal shears and eddies near promontories and estuaries and the generation of higher tidal harmonics. Nevertheless, whatever mechanism makes up the internal losses, we are confident that our estimates of the power flux across the boundaries (table 3) correctly represents the loss to the oceanic M_2 tidal system.

(*d*) *Numerical model for north Shetland seas*

In defining the tides along the northern part of the shelf, we were concerned whether the diffraction of tidal waves round the Shetland islands might require closely spaced measurements. The island mass is too large to be ignored, but most computer simulations oversimplify it as occupying only one or two grid areas. We therefore constructed a relatively simple numerical model, with grid-size fine enough to accommodate the northern half of the islands with fair realism and extending far enough into the open sea for the tides at the boundary to be defined adequately by interpolation between a few pressure stations. The grid size of about 6 km and its orientation was chosen to fit the island boundaries optimally. The boundary was taken as a trapezoid with corners at stations S5, 7, 8 and S10, and with data from Foula and Out Skerries completing the southern boundary (figures 8*a*, *b*). Apart from the two island stations just mentioned we used no data from the Shetland coast itself.

Frictional stress is fairly small in this area, so we used the linearized form quoted in § 6 (*b*), (7). This enabled us to use the now old-fashioned method of solution of the dynamical equations (Hansen 1948) in which the time-dependence is removed from the variables $\bar{u}$, $\bar{v}$, ζ and an elliptic set of equations is solved for their spatial dependence over the grid. The well-known equations are

$$\left.\begin{aligned} (\mathrm{i}\omega - k\bar{c}/h)\, u_0 + fv_0 &= g(\partial/\partial x)\,(\zeta - \zeta_e)_0, \\ (\mathrm{i}\omega - k\bar{c}/h)\, v_0 - fu_0 &= g(\partial/\partial y)\,(\zeta - \zeta_e)_0, \\ \partial u_0/\partial x + \partial v_0/\partial y &= \mathrm{i}\omega h^{-1}\zeta_0, \end{aligned}\right\} \tag{12}$$

where ω is the harmonic frequency, k and $\bar{c}$ are as in (7), and the suffix 0 denotes removal of a factor $\exp(-\mathrm{i}\omega t)$ from $\bar{u}$, $\bar{v}$, ζ. In brief, equations (12) expressed in finite differences were solved at all internal grid points, while at coastal boundaries the current component normal to the coast was set equal to zero and at open boundaries ζ_0 was defined. Solutions were obtained for a range of values of the linear friction coefficient k, and that which gave roughly the best values u_0, v_0 in comparison with the known currents was adopted. $k = 0.0025$ was satisfactory for semi-diurnal tides, but $k = 0.005$ was more appropriate for diurnal tides, even with the same value of $\bar{c}$, the mean ambient current, taken to be $0.2\,\mathrm{m\,s^{-1}}$. In all adopted solutions, the tidal elevation and phase at Baltasound, the only checkpoint on the coast, were found to agree fairly with the observed values (appendix B).

PHILOSOPHICAL TRANSACTIONS OF THE ROYAL SOCIETY A MATHEMATICAL, PHYSICAL & ENGINEERING SCIENCES

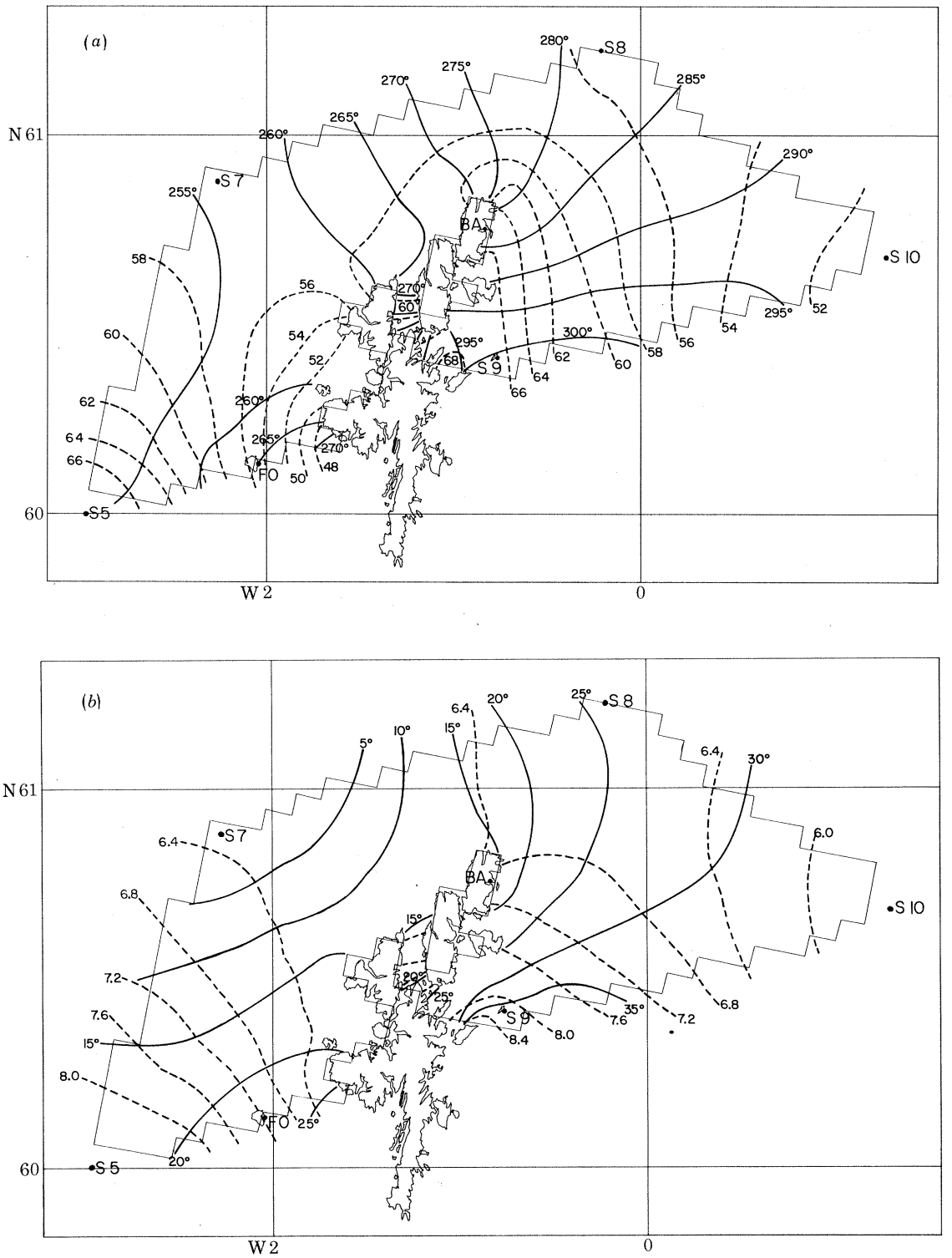

FIGURE 8. Cotidal maps for (*a*) M_2 and (*b*) O_1 in north Shetland area computed from external boundary data. Amplitude is in millibars; phase lag is in degrees.

PHILOSOPHICAL TRANSACTIONS OF THE ROYAL SOCIETY A MATHEMATICAL, PHYSICAL & ENGINEERING SCIENCES

The resulting cotidal maps for the M_2 and O_1 constituents are shown in figures 8*a* and 8*b* respectively. Maps for S_2 and K_1 are similar in appearance. We need not comment on their detail, but they both confirm a considerable disturbance round the islands which one could hardly deduce from a few coastal measurements. The chosen offshore stations do however show a smooth progression of tidal characteristics that appear to be reasonably typical of the conditions on the shelf as seen from the ocean. The gradients of the cotidal lines for M_2 near the corners of figure 8*a* agree reasonably well with those indicated in figure 7*a*, which is based on independent data. It is also interesting to note from figure 8*b* that the diurnal tides have a normal progression of phase and amplitude in this area, unlike the St Kilda régime and other shelf areas discussed in the following section.

(*e*) *Diurnal anomalies*

Figure 7*b* shows the vector gradients of the amplitude and phase of the K_1 constituent, deduced from the recorded currents as described in §6(*b*). The scale of the amplitude gradient vectors is ten times that used for M_2 in figure 7*a*, because of the generally smaller diurnal currents, but the scale of the phase gradient is the same as before.

The increase of diurnal amplitude away from the west Scottish coast is in striking contrast to the case for M_2. It is a result of the combination of a continental-shelf wave and a Kelvin wave, which are both possible wave modes at diurnal frequencies at this latitude, as explained by Cartwright *et al.* (1980). A year's pressure record at Scolpaig Bay, North Uist confirmed the marked reduction in diurnal amplitude at the Hebridean coast (O_1, 33 mm; K_1, 48 mm) compared with Hirta, St Kilda (O_1, 71 mm; K_1, 99 mm) – see appendix B. The combined wave at frequency ω:

$$H(x,y)\exp[-\mathrm{i}\omega t+\mathrm{i}G(x,y)]$$

can be expressed by

$$H\exp(\mathrm{i}G)=a'H_{\mathrm{K}}(y)\exp(\mathrm{i}m_{\mathrm{K}}x+\mathrm{i}G')+a''H_{\mathrm{s}}(y)\exp(\mathrm{i}m_{\mathrm{s}}x+\mathrm{i}G''), \tag{13}$$

where on the right side, suffixes K and s refer to Kelvin- and shelf-wave modes, $H_{\mathrm{K}}(y)$,$H_{\mathrm{s}}(y)$ are wave forms normal to a straight coast $y=0$ with $H_{\mathrm{K}}(0)=1$, $H_{\mathrm{s}}(0)=1$, and m_{K}, m_{s} are their associated longshore wavenumbers, all calculable for an assumed uniform shelf profile $h=h(y)$, (see §7*a* and Cartwright *et al.* 1980 for details). The observed elevations and phases at Hirta and Scolpaig Bay enable the arbitrary constants a', G', a'', G'' to be assigned. For the K_1 tide, these are

$$a',G'=131\,\mathrm{mm},\,138^\circ;\quad a'',G''=110\,\mathrm{mm},\,338^\circ \tag{14}$$

with wavenumbers $m_{\mathrm{K}}=[0.03\,\mathrm{deg\,km^{-1}}$, $m_{\mathrm{s}}=0.53\,\mathrm{deg\,km^{-1}}]$ both being positive, indicating northward propagation along the shelf.

From the above figures, one sees that the Kelvin wave has a somewhat larger amplitude, but the shelf wave effects a great reduction in total amplitude near the coast at $y=0$ owing to the phase difference of 200°. The character of the combined wave is best seen in the cotidal map corresponding to (13, 14), drawn in figure 9. The 200 km extent of x covers roughly the span of the Hebridean island chain with $x=0$ corresponding to North Uist. In the y-direction, the 200 m shelf break occurs at $y=110$ km and deep water at 2000 m begins at $y=150$ km. Over the near-shore part of the shelf the structure is dominated by the higher wavenumber shelf-wave, which produces the aforementioned shoreward decrease in amplitude and rapid changes of phase. It is interesting to note that the phase progression on the left of the origin is actually

southwards, again on account of the local antiphase condition of the two wave forms. Further north (large x) the phase advances northwards and the amplitude begins to increase shoreward for all y, but that is probably outside the range of validity of the model. In the area of figure 9, amplitude reaches a maximum near the shelf break, and from there decreases slowly into the ocean under the sole influence of the Kelvin wave, with a gentler progression of phase.

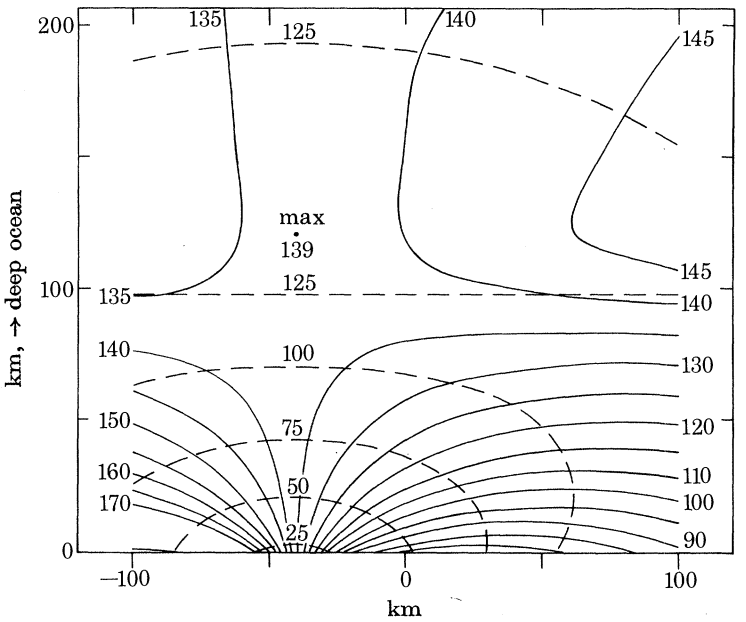

FIGURE 9. Idealized cotidal map for K_1 on St Kilda shelf area combining Kelvin wave and shelf wave (equation (13)). x axis is roughly northward along shelf. Amplitude is in millimetres; phase lag is in degrees.

The stations west of Scotland represented in figure 7*b* correspond roughly to $y = 65$ km. The oceanward gradient of H rotating from southwest to northwest, and the phase gradient rotating from southeast to northwest as one progresses from south to north, are all represented in figure 9. Other features illustrating the validity of the model are detailed in Cartwright *et al.* (1980).

We do not wish to suggest that the idealized form (13) gives an accurate cotidal map geographically, but it illustrates how high wavenumber structure can occur in the diurnal tides on the shelf. This greatly complicates the construction of diurnal cotidal maps near the shelf edge and makes coastal data especially unsuitable for use as boundary conditions for oceanic models that do not resolve the details of shelf bathymetry.

Attention has been focused on the west Scottish shelf because of the large diurnal inequality in its tidal streams, which first called attention to the existence of shelf waves (Cartwright 1969). We have not observed similar diurnal inequality in the currents in other parts of the shelf, and indeed the diurnal behaviour around Shetland has been shown to be normal (figure 8*b*). The northerly gradient of H between Shetland and Norway in figure 7*b* is related to another near-amphidrome in the North Sea southwest of Norway as in the case of M_2. There are some indications of complicated structure on the Faeroes Bank (top of figure 7*b*) which may possibly reflect a continuation of the Hebridean shelf system. Huthnance (1974) has discussed a possible system of rotating diurnal shelf-waves on Rockall Bank, suggested by some current measurements by J .W. Ramster (1970 Int. Coun. Explor. Sea CM1970/C: 25, 4 pp. – unpublished).

The few gradient vectors shown in figure 7*b* for the Celtic Sea suggest some variability in direction but no large gradients. However, the elevations themselves do tend to have the peculiarity noted on the Hebridean shelf, that coastal amplitudes tend to be smaller than near the shelf edge, as table 5 shows. (The data are extracted from appendixes A and B: see figure 7*c* for station positions.) It would be difficult to explain this phenomenon otherwise than by involving a shelf-wave mode, but the coastal topography is too complicated for a simple two-dimensional model.

TABLE 5. COMPARISON OF DIURNAL CONSTANTS AT CELTIC SEA SHELF-EDGE AND COAST

station	H	$G(O_1)$	H	$G(K_1)$
D1	7.5	328	7.9	076
C1	6.8	327	7.1	074
Ouessant	5.9	324	6.9	078
C3	6.8	329	6.8	101
Scilly	5.8	342	5.7	101
C6	7.1	334	7.6	112
P. Magee	5.7	304	7.7	065

7. OCEAN TIDES

(*a*) *East–west profiles*

As a first approximation, the tides of all species (except species 0) in the northwest Atlantic Ocean behave like Kelvin waves rotating around the main basin, trapped against the surrounding continental shelves, in our case the western European shelf. It is therefore interesting to compare the profile of amplitude of the principal constituent waves normal to the shelf edge, along our central line of stations at the latitude of 53.6°, with theoretical topographically trapped wave forms. Such wave forms are shown in figure 10, computed to satisfy the wave equations for a depth profile uniform in the north–south (x) direction with no flow normal to the profile at $y = 0$. The depth profile, which is also shown, was taken to be that at 53.6°, but of course the true bathymetry varies considerably north and south of that latitude.

The wave forms were computed by our colleague John Huthnance by a method due to M. S. Longuet-Higgins, which was also used for our analysis of the tides on the Hebridean shelf (§ 6*e*). In brief, the elevation ζ_0 is chosen to satisfy (Huthnance 1975)

$$\frac{\partial P}{\partial y} = K(y)\,\zeta_0, \quad \frac{\partial \zeta_0}{\partial y} = \frac{P}{h(y)}, \tag{15}$$

where

$$K(y) = kf\omega^{-1}\frac{\partial h}{\partial y} + k^2 h + \frac{f^2-\omega^2}{g} \tag{16}$$

is defined for the given frequency ω and wavenumber k as in an assumed factor $\exp \mathrm{i}(kx-\omega t)$. The equations (15) are integrated from a deep ocean condition which ensures a negative exponential form at large y, for various values of k, ultimately determining that value which satisfies the condition of zero flux at $y = 0$, namely

$$B(k) \equiv P - hkf\omega^{-1}\zeta_0 = 0. \tag{17}$$

For the tides of species 2, only one solution is possible, corresponding to a Kelvin wave when h is constant, but the tides of species 1, having $\omega < f$ at this latitude, have in addition a solution of higher wavenumber k corresponding to a continental shelf wave. Finally, for the curves shown

in figure 10 a constant complex multiplier was derived for each solution ζ_0 to provide a best fit to the measured amplitudes and phases at our stations along this section (figure 1 and appendixes A, B).

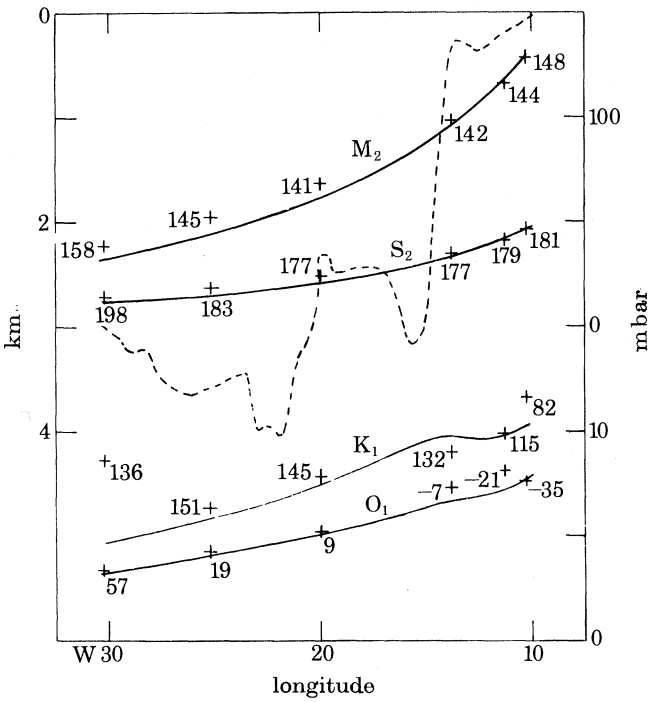

FIGURE 10. Tidal amplitudes for O_1, K_1, M_2, S_2 along 53.5° parallel west of Inishbofin. ——, Calculated profiles for bottom topography (– – –). +, Measured amplitude with phase lag (deg) indicated by number.

Data amplitudes are represented by crosses with the data phases written beneath them. For the semi-diurnal tides M_2 and S_2, the single Kelvin-type wave assumes a constant phase along the section and the observed phases are indeed within a few degrees of constancy. The observed amplitudes lie very close to the theoretical curve. Their tendency to lie above the curve at the stations furthest from the shelf probably results from the influence of the southbound Kelvin wave attached to the Canadian shelf, as are also the somewhat larger phases at the 30° W station.

The two-wave mix for the diurnal tides O_1 and K_1 allows some changes of phase, especially in the shelf region. The amplitudes do not fit the curves quite as well as for the semi-diurnals, but this is understandable on account of the greater sensitivity of the shelf-wave to topography, including its variations north and south of the section. Further out, the O_1 data fit the curve remarkably well, but the K_1 data at 30° W are quite anomalous. The K_1 anomaly most likely results from the influence of the mid-Atlantic ridge, which will have a larger topographical effect on the diurnal tides than on the semi-diurnal, but which is not properly included in our calculations. It will be seen that the cotidal map for K_1 is more complicated than that for O_1, again suggesting that topographical effects on the diurnal tides are extremely sensitive to small changes of frequency.

(*b*) *Comparison with computed tides*

Before presenting our cotidal maps, we examine some of our oceanic data in the context of information available from cotidal maps for the world's oceans computed by various authors.

Such maps have been computed by many different methods, varying principally in their treatment of friction, their constraint or lack of constraint to fit coastal data, and their allowance or non-allowance for the elasticity of the Earth and the self-attraction of the tidal bulges. Their results differ, of course, and it is useful to consider what degree of advantage we have in possessing the only correct solution for a certain oceanic zone. Scientists who compute world cotidal maps usually express little interest in the North Atlantic Ocean, because the general pattern of its tides is well established and there are many other parts of the world where the pattern itself is controversial or unsupported by tidal data of any sort. Nevertheless, it will be found that relatively few computed maps are consistently close to the measured tides in the North Atlantic Ocean.

TABLE 6. COMPARISON OF DATA WITH MAPS AT
(i) 60° N, 29° W; (ii) 45° N, 28° W

	(i)			(ii)	
	H/cm	G/deg		H/cm	G/deg
			M_2		
measurements	69	183		41	089
Gordeev *et al.* (1977)	25	190		24	330
Estes (1977)	25	230		25	070
Accad & Pekeris (1978)	25	230		23	075
Parke & Hendershott (1979)	70	185		50	092
Schwiderski (1979)	65	190		45	080
Zahel (1978)	75	225		20	075
†Zahel (1977)	65	145		55	045
			S_2		
measurements	27	222		12	112
†Bogdanov *et al.* (1973)	27	235		6	180
†Estes (1977)	17	225		14	108
Accad & Pekeris (1978)	10	255		7	090
Parke & Hendershott (1979)	39	230		15	145
			K_1		
measurements	11	137		5	107
†Bogdanov *et al.* (1973)	9	145		3	110
†Estes (1977)	9	135		4	095
Parke & Hendershott (1979)	9	135		4	110
Zahel (1978)	10	100		5	060
			O_1		
measurements	5	066		2	010
†Bogdanov *et al.* (1973)	4	085		3	345
†Estes (1977)	5	125		3	090

† Computations for a rigid Earth.

It would be impractical to make a pictorial comparison of the various representations of our area. We have instead selected two positions well remote from land, at which we have tidal data, and have taken the readings at these points from various cotidal maps for comparison. These positions are (i) 60° N, 29° W and (ii) 45° N, 28° W, very close to D9 and M4 respectively. Table 6 shows the measured elevation H/cm and phase lag G/deg for the major diurnal and semi-diurnal constituents at these positions, and the corresponding readings taken with due care and interpretation from the named publications. (Some maps confuse 'range' with 'amplitude'; others confuse lunar hours with lunar half-hours.) Phases in lunar hours were multiplied by 30 to give the phases in degrees.

Comparisons were made wherever possible with results of calculations that allow for elasticity and self-attraction, but some results for a rigid Earth were included where indicated by a † sign, to make a fair number. Zahel's (1977) map for a rigid Earth was added to the list for M_2

because its fine 1° mesh might be thought to compensate partially for its absence of elastic effects. Dr Schwiderski is known to be preparing elastic–Earth cotidal maps for S_2, K_1 and O_1, but his results are not available to us at the time of writing.

Obviously there are considerable variations, but it would not be fair to judge the general accuracy of any global cotidal map on the basis of its readings at these two positions alone. For M_2, the first three pairs of map readings are surprisingly similar in their very low amplitude, suggesting similarity of computation, leading to a too easterly position for the amphidrome. Gordeev *et al.* (1977) place the amphidrome at about 25° W, which is certainly wrong. We used the maps of Accad & Pekeris (1978) corresponding to 'sloping shelf' boundaries and unsmoothed coastlines, but their maps for other conditions give rather similar results. Another similar pair is Parke & Hendershott (1979) and Schwiderski (1979 U.S. Navy Surface Weapons Centre, Dahlgren, Virginia, 78 pp. – unpublished), who both give reasonably accurate results for M_2. Parke & Hendershott's results for S_2 are less successful, but their results for K_1 are very good. The other sets of results are too variable to call for any summarizing comment.

The main conclusions we wish to draw from table 6 are first that computed representations of the tides in the northeastern Atlantic are not as perfect as some authors seem to imply; secondly, that any cotidal map which is within 10% in H and 5° in G compared with the true values is likely to give a more accurate representation of the tides in our area than any presently existing cotidal map.

(*c*) *Cotidal maps – diurnal*

Given our two complete circuits of measured boundary data, the modern tendency would be to use a numerical model to fill the interior. We have avoided this approach, partly because our colleague Dr R. A. Flather is working on the technique of a combined shelf-cum-ocean numerical tidal model for the area, and partly because any model applies physical and numerical constraints the validity of which is still controversial. We prefer to interpolate between the boundary data by the intelligent drawing of smooth curves, and leave it to others to use the data set as a testing ground for various numerical formulations. A similar approach has been made by Luther & Wunsch (1975) to the island tidal data of the central Pacific. From the last section, we are confident that our hand-drawn maps will be as good as or better than any previous maps of the area.

Figures 11*a*, *b* show our estimated cotidal maps for O_1 and K_1 respectively. These were harder to draw than the semi-diurnal cotidal maps because of the complicated shelf structure discussed in §6(*e*), but similar difficulties would be encountered by numerical models, that furthermore would hardly allow for the considerable standard errors in some of the diurnal data (appendix A). We have represented shelf structure only when supported by sufficiently dense data points as in the southwest Celtic Sea, where some reliable boundary data closer to the shores are also given by Robinson's (1979) maps. Near the entrance to the North Sea, our north Shetland computations, §6(*d*), afforded some guidance. We have not attempted to draw detail close to the Hebrides or the Faeroes, but there is enough information from station R3 to suggest deflection of the co-phase lines over Rockall Bank.

The maps for O_1 and K_1 differ considerably in appearance. This difference is largely a result of the swing from a phase difference of about 120–130° in the south and east to 50° or less in the vicinity of Iceland, as was pointed out in §5(*b*) in connection with figure 5. The change in tidal age is manifest in a large zone of stationary phase and maximum amplitude of about 11 mbar† – an

† mbar = 10^2 Pa.

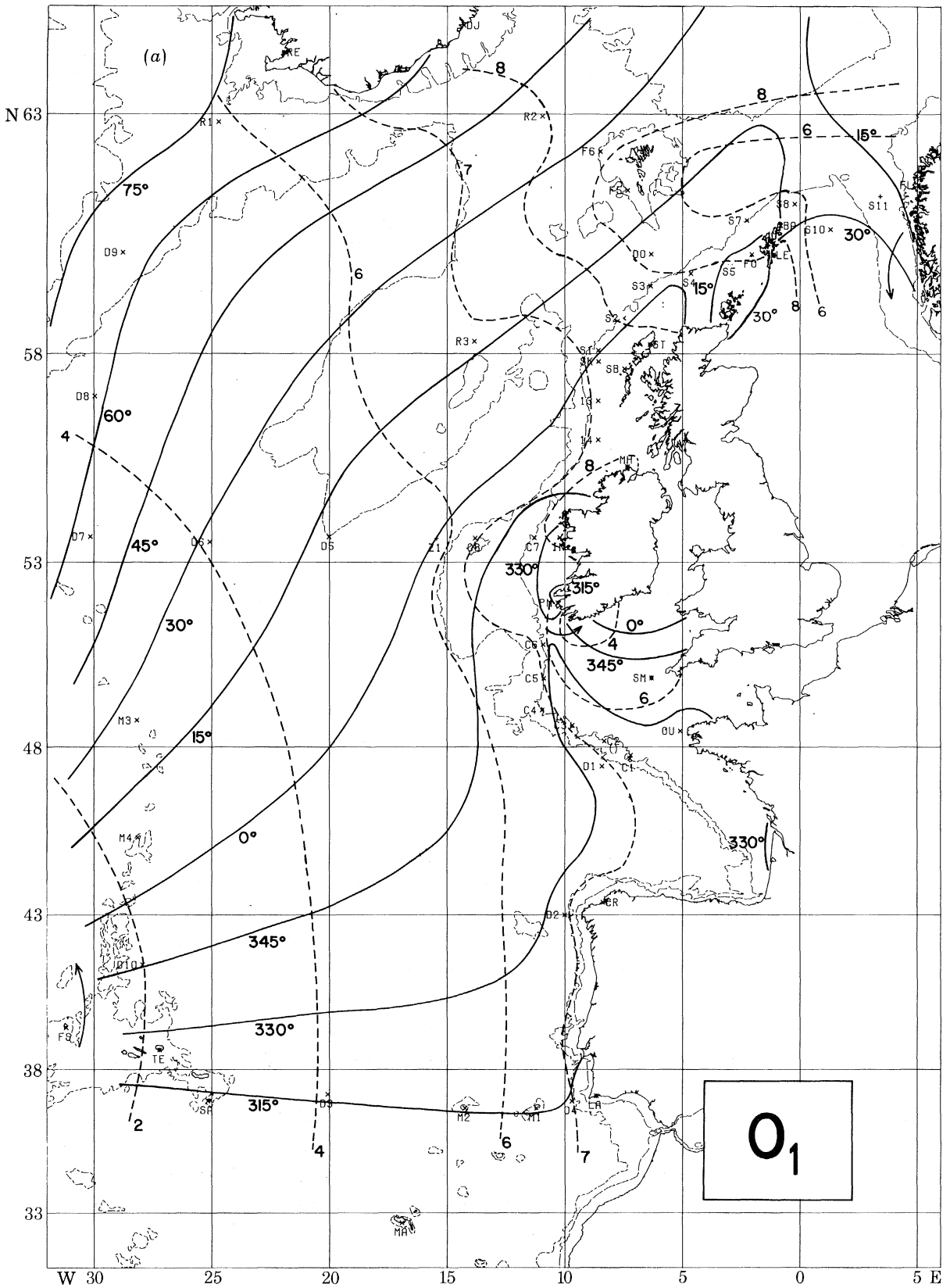

FIGURE 11 (*a*). For legend see facing page.

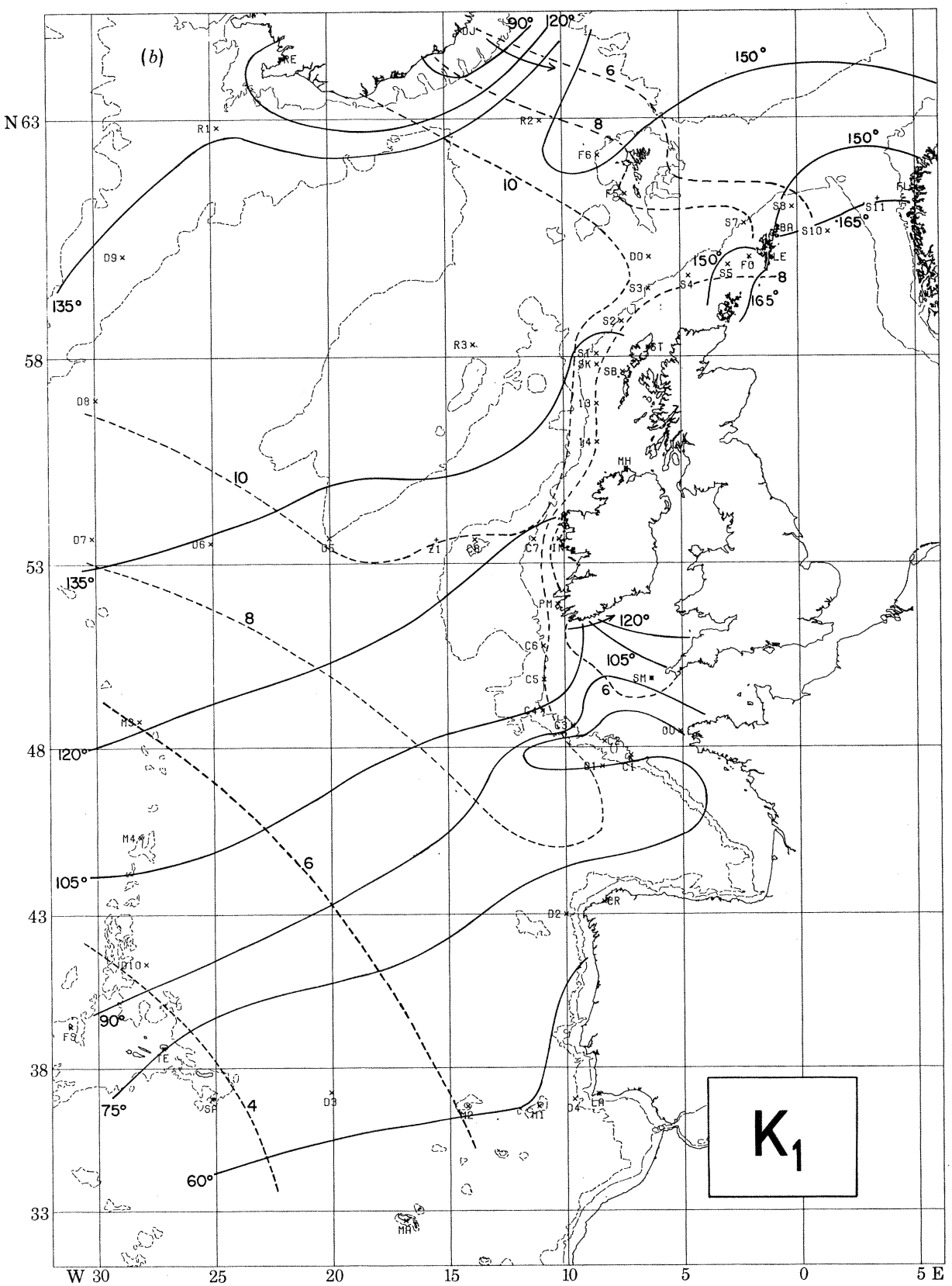

FIGURE 11. Oceanic cotidal maps. ——, Phase lag in degrees; – – –, amplitude in millibars. →, sense of phase progression round probable amphidromes.

'anti-amphidrome' – in the K_1 map centred on the deep trough between Rockall Bank and Reykjanes Ridge, and by absence of any similar behaviour in O_1. (The recorded amplitude at Rockall (R3) being only 9 mbar, suggests some structure inside our 10 mbar contour, to represent which we do not have enough detail.) The anti-amphidrome should produce a relatively large anomaly in the K_1 loading tide in southern Iceland, relative to O_1. Another difference is the suggestion of a K_1 amphidrome somewhere northwest of Iceland. Such an amphidrome appears in the computed map for K_1 by Estes (1977) but not in that by Parke & Hendershott (1979).

Although our area clearly does not embrace the principal diurnal amphidrome region of the central north Atlantic, there is sufficient convergence of the co-phase lines and progressive reduction in amplitude in the southwest corner of both maps to give a good idea of where their amphidromes lie. We estimate 40° N, 37° W for the O_1 amphidrome, 32° N, 35° W for K_1. Estes' maps make both K_1 and O_1 amphidromes appear at about the same latitude (35° N) and further west than our positions. Parke & Hendershott's position for the K_1 amphidrome (30° N, 40° W) is closer to our extrapolation for K_1. Zahel's (1978) position for the K_1 amphidrome appears to be about (45° N, 45° W), too far northwest, but the 4° resolution of his grid does not favour precise positioning.

(*d*) *Cotidal maps – semi-diurnal*

Figures 12*a*, *b* show our drawings for M_2 and S_2 respectively, following the principles discussed in the last section. The contours are drawn at intervals of 20 mbar (M_2), 10 mbar (S_2), and 30°, except for additional co-phase lines at 170° (M_2) and 200° (S_2) that occur in places that otherwise show little detail. For this tidal species some guidance as to shape of the cotidal lines in the region of the Bay of Biscay is afforded by the short pelagic pressure measurements made by the Centre Océanologique de Bretagne (Hyacinthe 1974). On the whole, these maps were much more straightforward to interpolate than the diurnal maps because of smoother behaviour along the shelf edge and very small sampling errors in the data. The only area where a good deal of subjective interpretation was required was between the Faeroes and southeast Iceland, where a few more pelagic records would have helped to resolve the detail associated with the nearby amphidrome manifestly present in both constituents.

This amphidrome east of Iceland appears in all computed maps for the semi-diurnal tides except those of Bogdanov *et al.* (1973) who probably over-simplify their boundary conditions in that region. Our placement of the nodal position is a little conjectural in the absence of data north of Djupivogur, but the position agrees in some respects with that of Accad & Pekeris (1978) rather than that of Parke & Hendershott (1979), which is certainly a little too far south. This amphidrome should not be confused with the low amplitude at Thorshavn on the west coast of the Faeroe Islands (appendix B), because our measurements to the west of the Faeroes are inconsistent with a major amphidrome centred on the Faeroes as a whole. (See also § 6 (*b*).) Lack of data prevents us from representing the probably small-scale structure east of the Faeroes.

As with the diurnal tides, the principal semi-diurnal amphidromic region is outside our circuit of measurements, but the convergence of the co-phase lines shows it to be well north of the corresponding diurnal amphidromes. Being fairly close to the region defined by our westernmost stations D6, D7, M3, we may estimate the positions of the M_2 and S_2 amphidromes by linear extrapolation from the constants at these stations. Following the principle suggested by Cartwright (1971), that the quantities $H\cos G$ and $H\sin G$ vary smoothly in space, we assign complex constants A, B, C so that for a given constituent

$$H_1 + \mathrm{i}H_2 = H\exp(\mathrm{i}G) = Ax + By + C \qquad (18)$$

fits the data values from at least three stations in the vicinity. The condition $Ax + By + C = 0$ then defines two lines in (x, y) space the intersection of which determines the amphidrome.

In the present case, the following equivalent procedure is perhaps more heuristically appealing. We already have partial loci for $H_1 = 0$ and $H_2 = 0$ in the co-phase lines for 90° and 180° respectively, and their linear extension may be estimated by extrapolating values of $H\cos G$ and $H\sin G$ along the line D5–D7 at 53.6° N latitude. For M_2, linear extrapolation at this latitude gives zeros at 50.5° W (H_1) and 35.3° W (H_2). Connecting the existing loci to these points then makes the amphidromic position (50° N, 39° W). For S_2, a similar procedure gives (50° N, 36° W). The slight easterly shift from M_2 to S_2 is in accordance with the results of all those who have computed both positions by the same method; the absolute computed positions vary as discussed in § 7(*b*).

TABLE 7

	$G(M_2)$	$G(S_2)$	difference
Madeira	44	65	21
	60	85	25
	90	120	30
	120	155	35
	150	190	40
	180	220	40
St John's	317	361	44

In the North Atlantic Ocean as a whole, north of about 35° N, the semi-diurnal tide appears to travel as a sort of Kelvin wave rotating counter-clockwise about the amphidromic region, from Europe past Iceland to the North American coast. In a progressive wave through a nonlinearly dissipating medium one expects the dissipative effect to be stronger in the higher frequency components, and since the dissipation is relatively weak this will be manifest in a greater rate of increase of phase lag for higher frequency. It is therefore interesting to observe the above increase in phase lag of S_2 relative to M_2 (a measure of 'age'), at selected points along the 60 mbar co-amplitude line for M_2, taken from figures 12*a* and 12*b*. The 'age' increases steadily to about the latitude of Ireland, then stays relatively constant. The last entry is for St John's, Newfoundland, which may be regarded as a later phase of the same progression; it shows a small increase on the previous age. Although this trend may be due to strong dissipation off the European shelf followed by weak dissipation round the northern sector, it is hard to relate the change in age between the top three (southernmost) entries in table 7 to the strong dissipation off the English Channel. An unidentified dissipating mechanism off the Iberian peninsula or on the Biscay shelf might be suggested, and this is supported by the results of the following section.

(*e*) *Currents and power flux*

Having produced what appear to be reasonably accurate cotidal maps for the semi-diurnal constituents, we reversed the procedure of § 6(*b*) to deduce the depth-mean or 'barotropic' tidal currents from the pressure gradients defined by the maps. To do this, we essentially solved equations (6) for $\bar{u}$, $\bar{v}$, setting $F/h = 0$ and using spherical coordinates in place of x, y. If the time factor $\exp(-i\omega t)$ is omitted the equations are

$$\left.\begin{aligned} \bar{u} &= ga^{-1}(i\omega\chi_\theta - 2\Omega\tan\theta\ \chi_\phi)\ (4\Omega^2\sin^2\theta - \omega^2)^{-1}, \\ \bar{v} &= ga^{-1}(2\Omega\sin\theta\ \chi_\theta + i\omega\sec\theta\ \chi_\phi)\ (4\Omega^2\sin^2\theta - \omega^2)^{-1} \end{aligned}\right\} \quad (19)$$

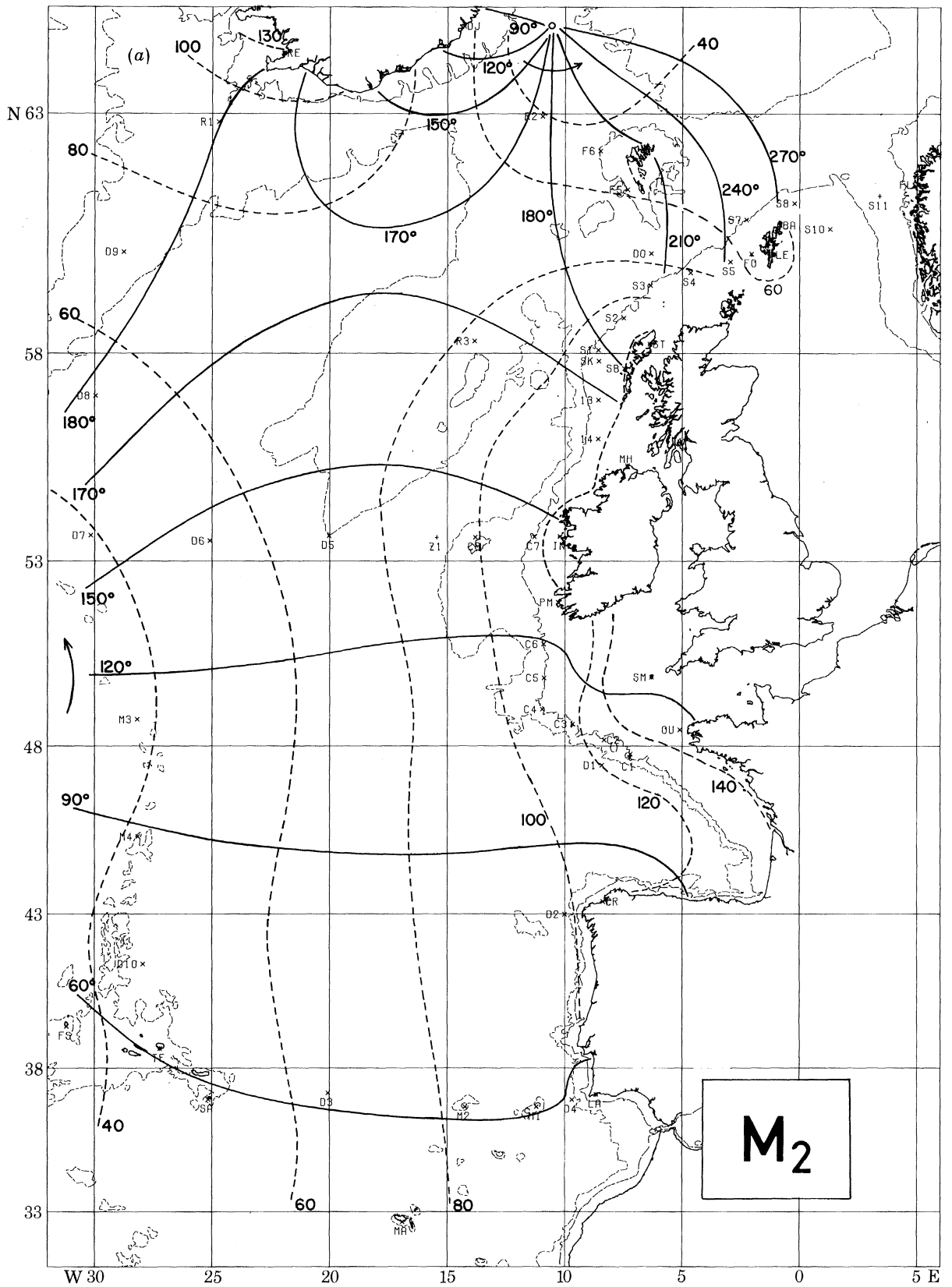

FIGURE 12 (a). For legend see facing page.

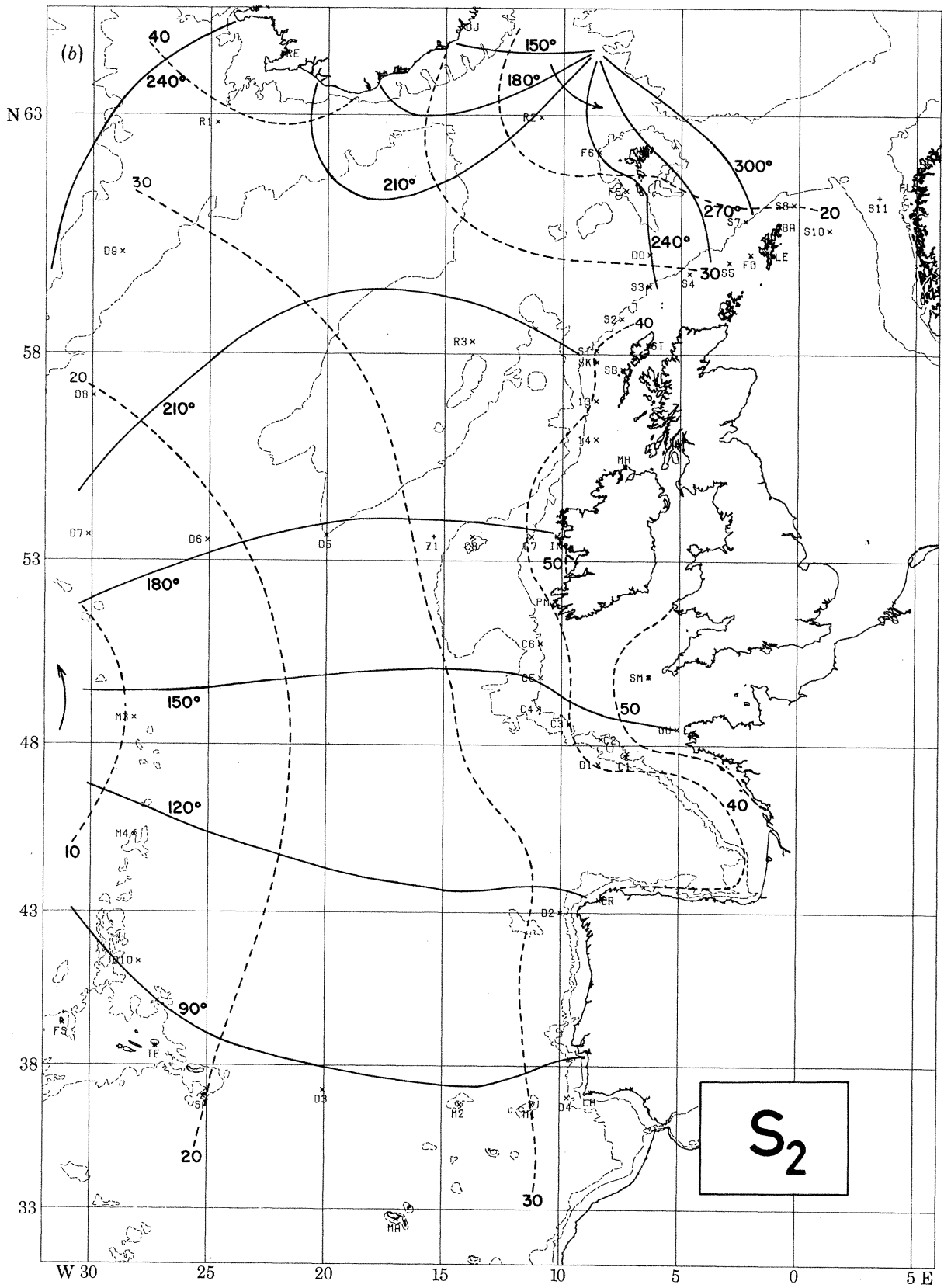

FIGURE 12. Oceanic cotidal maps. ——, Phase lag in degrees; – – –, amplitude in millibars.

PHILOSOPHICAL TRANSACTIONS OF THE ROYAL SOCIETY A MATHEMATICAL, PHYSICAL & ENGINEERING SCIENCES

where

θ, ϕ are the north latitude, west longitude,

a, g are the local Earth's radius, local gravity,

$$\chi = \zeta - 0.69\zeta' - \zeta'',$$

$$\zeta' = A_1 \xi^2 \sin 2\theta \exp(\mathrm{i}\phi), \text{ for diurnal tides,}$$

$$A_2 \xi^2 \cos^2\theta \exp(2\mathrm{i}\phi), \text{ for semi-diurnal tides,}$$

$$\xi = a/(\text{equational radius}),$$

$$A_1 = 0.1013\,\mathrm{m}\ (\mathrm{O}_1),\ 0.1425\,\mathrm{m}\ (\mathrm{K}_1),$$

$$A_2 = 0.2441\,\mathrm{m}\ (\mathrm{M}_2),\ 0.1136\,\mathrm{m}\ (\mathrm{S}_2)$$

and suffixes denote differentiation.

We derived gradients of ζ by digitizing the cotidal maps, figures 11, 12, at an array of 14×9 points spaced at 2° in θ from 37° to 63° N and at 2.5° in ϕ from 10° to 30° W. Central differences of $H\cos G$ and $H\sin G$ across 4° in θ and 5° in ϕ were then used to define ζ_θ and ζ_ϕ at an array of 12×7 points, omitting the former boundary points. A constant mean sea-water density of $\sigma_t = 28$ was assumed in converting from pressure to tidal elevation.

The loading potential $g\zeta''$ is usually omitted from such calculations but here we used a digitized array from a map supplied by M. E. Parke (personal communication) as derived from the tidal solutions presented in Parke & Hendershott (1979). As shown by those authors, ζ'' is comparable with the equilibrium tide $0.69\zeta'$, but having spatial structure similar to the ocean tide ζ its gradients are in places greater than those of ζ' if on a smaller spatial scale. In general, the tidal potential plays a more important role in calculations for the ocean than for the shelf seas because of the smaller gradients of ζ in the ocean. Omitting ζ'' was found to make differences of order 20% in some of the calculated currents.

Figure 13*a* shows the results of the calculations described above for the M_2 tide, in the form of oriented axes of the current ellipses corresponding to $(\bar{u}, \bar{v})$, with sense of rotation indicated by c if clockwise, at each of the 84 interior grid points. Also shown are vectors whose north and west components are respectively

$$\left.\begin{aligned} P_x &= \tfrac{1}{2}\rho g \bar{h}\,\mathrm{Re}\,(\bar{u}\chi^*)\, a\cos\theta\delta\phi, \\ P_y &= \tfrac{1}{2}\rho g \bar{h}\,\mathrm{Re}\,(\bar{v}\chi^*)\, a\delta\theta, \end{aligned}\right\} \tag{20}$$

where ρ is the sea density, $\delta\theta$, $\delta\phi$ are mesh increments in latitude and longitude, h is the suitably averaged depth over each mesh area, and * denotes the complex conjugate. P_x and P_y represent the mean power flux per tidal cycle crossing the sides of a mesh area in the directions of $\bar{u}$ and $\bar{v}$; they may be summed over a sequence of mesh lines to give the total power flux across the combined line.

Currents and power fluxes are obviously greatest in the northeast sector of the area as a result of the large pressure gradients, seen there in the cotidal map, (figure 12*a*) and the strong dissipation in the shelf seas round Britain. The largest computed major axis of a current ellipse is 0.19 m s^{-1} in a depth of about 2 km south of Iceland. This is of the same order as tidal currents experienced on the outer continental shelf in only 150 m depth. Remembering that this is the mean current over the whole water column, it represents an order of magnitude greater mass flux per horizontal width than, say, the tidal flow through the Strait of Dover. The tidal currents at specific depth may of course be greater or less than the barotropic flow, owing to the presence of internal tidal modes.

PHILOSOPHICAL TRANSACTIONS OF THE ROYAL SOCIETY A MATHEMATICAL, PHYSICAL & ENGINEERING SCIENCES

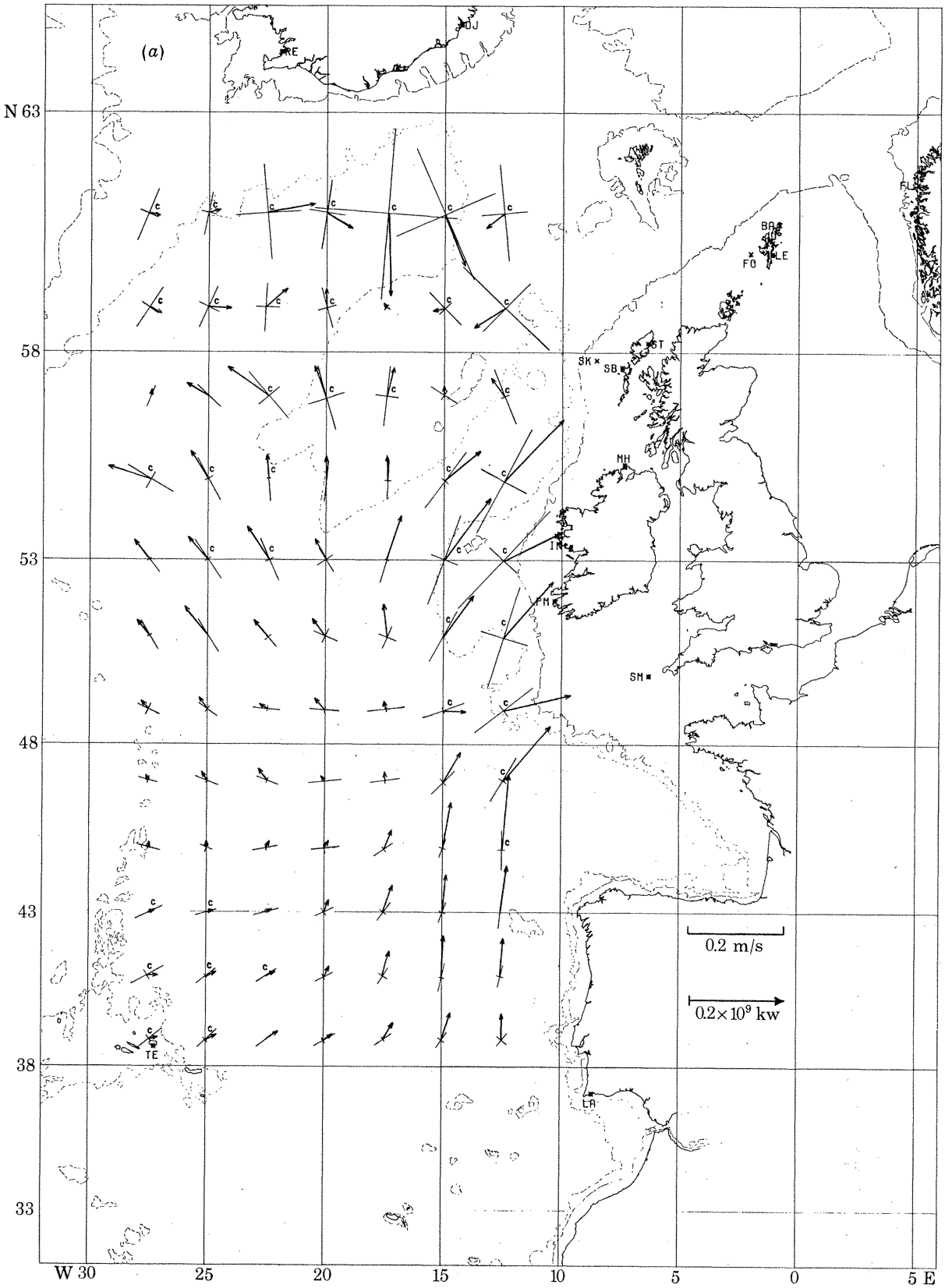

FIGURE 13. (*a*) Axes of tidal ellipses and power flux vectors (→) computed for M_2 cotidal map (figure 12*a*). c denotes clockwise rotation of current vector.

PHILOSOPHICAL TRANSACTIONS OF THE ROYAL SOCIETY A MATHEMATICAL, PHYSICAL & ENGINEERING SCIENCES

The power flux vectors are probably the most physically revealing feature of figure 13*a*. They clearly show a generally northward flux of energy being diverted towards the dissipating shelf region to the east and to a lesser extent following the general progression of the tidal wave clockwise round the amphidrome, presumably to other dissipating regions on the North American shelf. In the extreme north of the region the situation is more confused, with a tendency for power to enter the region, as it does also in the extreme south. It is instructive to consider the numerical values for the flux into and out of the whole area, that is, for the westward components across the eastern and western boundaries and the northward components across the southern and northern boundaries. These are detailed in table 8, and their salient features are sketched in figure 13*b* for convenience in the following discussion.

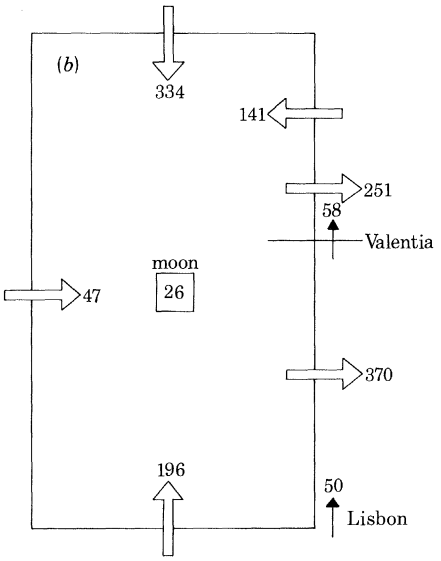

FIGURE 13. (*b*) Simplified M_2 power flux diagram, showing input to and output from the oceanic area mapped in figure 13*a*. Units are GW. The eastern boundary is divided into sections north and south of 52° N (Valentia), as discussed in the text.

TABLE 8. COMPONENTS OF M_2 POWER FLUX

	westward flux/GW			northward flux/GW	
lat./deg	east side	west side	long./deg	south side	north side
61	37	−27	12.5	50	−29
59	69	−26	15	58	−113
57	35	−2	17.5	35	−177
55	−122	93	20	18	−35
53	−129	28	22.5	14	20
51	−104	26	25	14	6
49	−134	12	27.5	6	−6
47	−101	3	total	196	−334
45	−11	−1			
43	−13	−14			
41	−7	−24			
39	1	−20			
total	−480	47			

The figures in the left half of table 8 represent the flux across consecutive 2° segments of the meridians at 11.25° W and 28.75° W respectively. Those on the right half represent the flux

across 2.5° segments of the latitude parallels at 38° N and 62° N respectively. Consider first the flux towards the shelf. Since the eastern boundary comes close to the Portuguese coast at Lisbon (38°) and southwest Eire at Valentia (52°), we may divide the flux components into those south and north of 52° N. The outward flux in the southern part adds up to 370 GW, and to this we should add an estimated 50 GW for the northward flux at 38° N between the rectangle's boundary and the Portuguese coast, and subtract an estimated 58 GW for the northward flux between the boundary and the Irish coast, making a total flux of 362 GW into the entire shelf region south of Eire. This is almost twice the value 183 GW of the flux into the Celtic Sea between Valentia and Ouessant, computed from the shelf boundary measurements by a similar integral (table 3). There are possible errors of, say, 5 % in both figures, but it seems difficult to avoid the conclusion that a great deal of tidal energy is dissipated along the shelf seas of western France, Spain and Portugal, which is invariably neglected in global calculations. Whether this is due to horizontal shear along the coastline or internal processes at the shelf edge is a subject for further investigation.

Consider now the eastward flux north of 52°. The total from table 8, with the addition of the estimated 58 GW flowing between the rectangle and Valentia, is 168 GW. This really consists of 309 GW fed into the shelf area between 52° and 56° and a partial return westward flux of 141 GW north of 56°. If we allow about 50 GW more to flow westwards between the top of the rectangle and southeast Iceland, this leaves about 120 GW being transmitted across a line joining Eire and Iceland, the transmission being confined to the shelf edge west and north of Eire. Evidently, the energy is trapped to follow the shelf contours, turning north of Scotland towards the Norwegian Sea, in accordance with the shelf-edge cotidal gradients (figure 7*a*). The 120 GW are again about twice the 60 GW being dissipated in the North and Scottish seas (table 3) as deduced from the shelf measurements, but here we have the possibility of continued transmission north of Norway and into the Arctic Ocean, so the imbalance is not as critical as in the Celtic Sea sector. In fact, there is probably some flow of tidal energy towards the Atlantic Ocean through the Denmark Strait between Iceland and Greenland, although the data are insufficient to give a quantitative estimate, so the total flow of tidal energy from the Atlantic into the Arctic seas may be fairly small.

Finally, it is interesting to consider the power flux into the rectangle itself. By adding all the totals in table 8 we obtain

$$(-480-47+196+334) = 3\,\mathrm{GW}$$

for the power transmission into the rectangle. This is remarkably small, considering the possible errors in each of the component figures, that also depend on rather arbitrary depth averages used in (20). However, there is also a substantial power input from the lunar gravitational forces themselves which may be fairly accurately computed from an integral similar to the second term on the right side of (10). This input is 26 GW, making a total of 29 GW to be dissipated within the 3.3×10^6 km^2 area of the rectangle. An oceanic rate of 9 kW km^{-2} is appropriately small compared with, say, about 330 kW km^{-2} for the North Sea, but if one multiplies it by the 360×10^6 km^2 of the world's oceans, one gets 3.2×10^3 GW which is about the total dissipation required to account for the lunar acceleration, without including the dissipation in the shallow seas (Lambeck 1977). Such a calculation is of course overweighted, because the tides in our area are on the whole larger than in most of the world's oceans, and in any case possible errors in the four numbers in parentheses above could easily halve the estimate of 9 kW km^{-2}. But these considerations do suggest a possible non-trivial contribution to the global dissipation from deep oceanic

PHILOSOPHICAL TRANSACTIONS OF THE ROYAL SOCIETY A MATHEMATICAL, PHYSICAL & ENGINEERING SCIENCES

areas, usually neglected. The only known physical mechanism for this is conversion of tidal energy to baroclinic modes, principally at the shelf edge, but quantitative estimates for this conversion rate have so far been rather small (Schott 1977). The physical reality of the horizontal eddy viscosity which accounts for a good deal of the dissipation in Zahel's (1978) models is again questionable, but it would merit further investigation.

(*f*) *Tests for mass continuity*

The currents discussed in the previous section were derived from the equations of momentum (19) without reference to the equation of mass continuity:

$$a^{-1}\sec\theta[(h\bar{u})_{\phi}+(h\bar{v}\cos\theta)_{\theta}]=\mathrm{i}\omega\zeta. \tag{21}$$

If (21) is satisfied at any point of the computational grid it implies that our hand-drawn cotidal map is identical with a complete solution of the tidal equations, which is unlikely to be the case in general. To test how far the equation of mass continuity was satisfied, we computed estimates of the left side of (21) by taking differences of the current flux components $(h\bar{u}, h\bar{v})$ computed by (19) across the four grid points surrounding each rectangle, and compared them with estimates of the right side of (21) formed by the average of the four values of ζ. Out of 66 such comparisons, about five gave fair agreement, another fifteen were within a factor of 2 in magnitude and 90° in phase; the rest showed no definable measure of agreement beyond a generally correct order of magnitude. We had hoped for better than this, but in retrospect the accuracy of a drawn cotidal map is greatly strained by taking double derivatives as implied by (19, 21). Further, with the relatively coarse grid of order 2°, differences in depth h between consecutive points were sometimes as large as a factor of 3 or 4, making simple calculation of flux differences in terms of the two end-values very dubious. A fair test of continuity of this sort would require a grid spacing of at most 0.5° with correspondingly detailed bathymetry, and we were not prepared to go to that amount of trouble.

(*g*) *Cotidal map for* M_3

The M_3 constituent of the tide is generally neglected because of its small amplitude. Nevertheless, it is a distinct harmonic component, linearly driven by a potential which is proportional to

$$\cos^3\theta\exp\mathrm{i}(3\phi-\omega_3 t),$$

where $2\pi/\omega_3$ is a third of a mean lunar day, that is a period of 8.2804 h. It lies in a part of the spectrum with fairly low noise level so that it may be extracted with little error from pressure records of about a month's duration. Robinson (1979) drew a cotidal map for M_3 in the Irish and northern Celtic Seas based on sea level and current measurements and that is probably the first published example. Huthnance (1980*b*) has studied an extraordinary magnification of the M_3 tide on the coast of Brazil.

The M_3 constants from our pelagic stations, backed up by published constants from several coastal ports (appendixes A, B) show smooth progressions of amplitude and phase even though amplitudes in the southern and western areas are generally less than 0.5 mb. Our cotidal map, drawn on the same principles as for the other constituents, is presented in figure 14. Whereas none of the diurnal or semi-diurnal cotidal maps contains an amphidrome within the prescribed area, figure 14 shows two amphidromes of opposite sense of rotation within the western boundary. This accords with a general principle suggested by mathematical studies of tides in basins, that

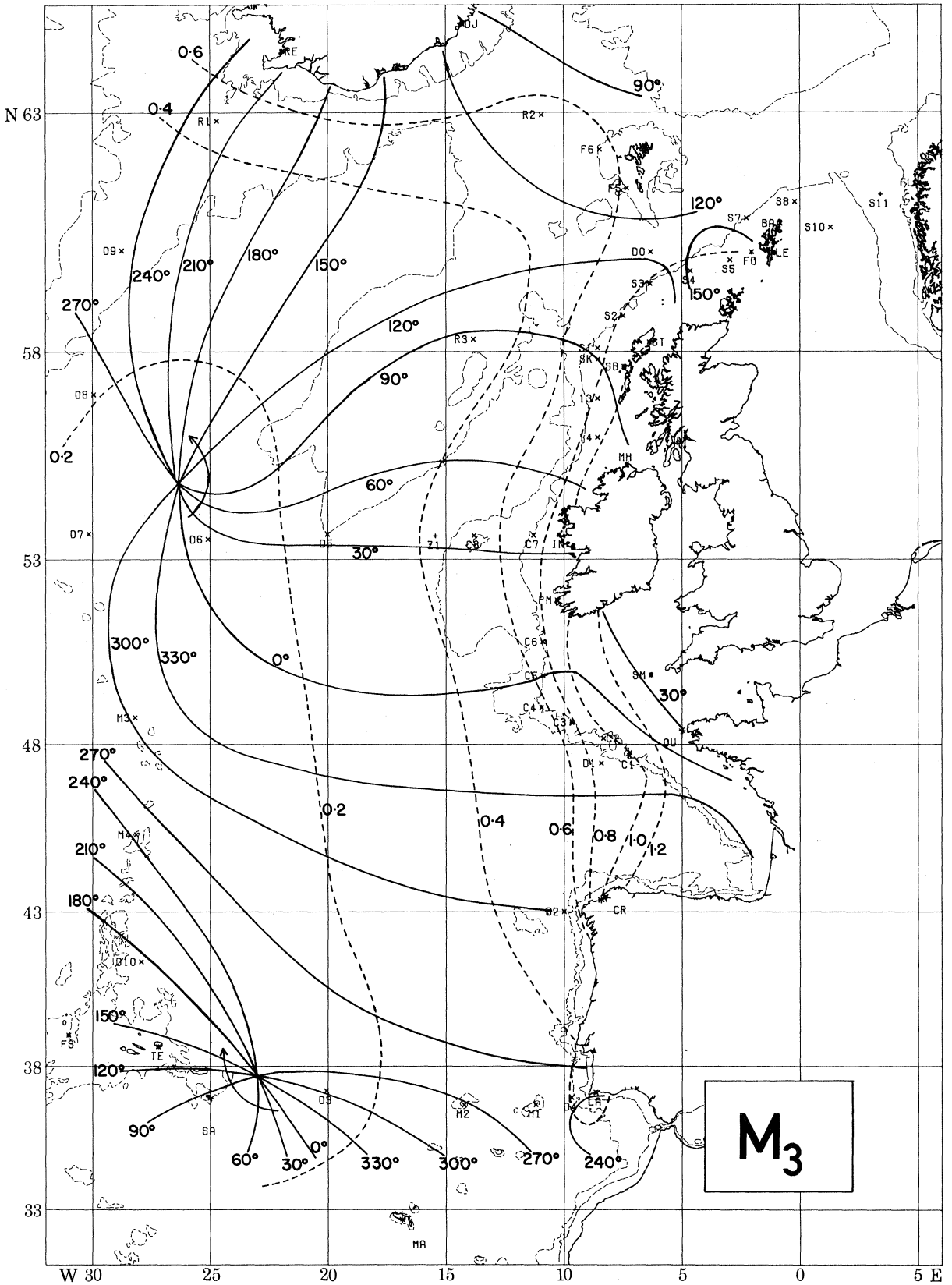

FIGURE 14. Oceanic cotidal map for M_3. ——, phase lag in degrees; – – –, amplitude in millibars.

PHILOSOPHICAL TRANSACTIONS OF THE ROYAL SOCIETY A MATHEMATICAL, PHYSICAL & ENGINEERING SCIENCES

for a given basin the number of amphidromes tends to increase with the frequency of the driving potential. The two amphidromes produce a large north–south elongated zone of very low amplitude in the western part of our zone. This makes some of the western stations rather imprecise in their phase estimates, but the general pattern of phases shown is well confirmed.

Large M_3 amplitudes are concentrated in the shelf seas between northern Spain and the Hebrides, where they are generally of order 1 mbar, or 10 mm in sea level. Amplitudes of 10 mm or greater are also general throughout the seas surrounding Britain excepting the extreme northern part of the North Sea. This is considerably greater than the 'equilibrium amplitude' of M_3 which at 50° N is about 0.7 mm. Similar magnifications for the somewhat related diurnal constituent M_1, which has a period of exactly one mean lunar day and is resolvable from other diurnal tides only with several years of data, are also observed to be concentrated in this sea area (Cartwright 1975, 1976*b*). It is arguable that the enhancement of M_1 is due to a spatial resonance of a normal mode of the Atlantic Ocean to the P_3^1 generating harmonic (Cartwright 1975), and it is possible, if unlikely, that a similar mechanism applies to M_3. Both constituents have amplitudes too great in deep-water locations to be accountable by nonlinear interactions with M_2.

8. Concluding remarks

We have for the first time completely defined by direct measurement the tidal conditions along the boundary of the shelf seas surrounding the British Isles and in the eastern half of the ocean west of Europe (excepting the Norwegian Sea). The measurements have been shown to differ considerably from most results of global numerical computations, and we have for the most part avoided the use of such computational methods in interpreting the data. The diurnal tides have proved to be the most difficult to map accurately because of their tendency to be trapped in short-wavelength modes along the shelf edges and other bathymetric features, but such modes have not been properly represented in numerical ocean tide models either. Despite these limitations, we have presented adequate oceanic cotidal maps of the constituents O_1, K_1, M_2, S_2 and M_3.

Direct estimates of tidal power flux into the shelf seas considerably exceed values previously assumed in global calculations, for example by Miller (1966). In the case of the North Sea and Scottish Seas they also greatly exceed our own estimate of the loss due to bottom friction. Our estimate of the power transmitted from the ocean to the shelf seas between Lisbon and Valentia is again much greater than that transmitted across the shelf between Ouessant and Valentia, suggesting further unidentified sinks of energy along the Biscay shelf. On the other hand, the power loss within our main oceanic area, about 9 kW km^{-2} is satisfactorily small, if somewhat greater than might be expected. These discrepancies between present and previous estimates of tidal power loss suggest that it may still be possible to reconcile the oceanic dissipation with estimates based on observations of the Moon and artificial satellites (Lambeck 1977), but to do this tidal surveys like the present one will have to be made in many other critical ocean-cum-shelf areas, and fuller investigations of the physics of shallow-sea tidal dissipation are needed.

Our investigations have taken ten years of intermittent effort, backed up by nationally funded research ships and an institutional policy that oceanic tidal research is scientifically worthwhile. As a result, we have surveyed about one one-hundredth part of the world's ocean surface. Our technology and experience have steadily progressed, so that a similar programme could nowadays be accomplished in about three years of concentrated effort. Even so, to make a significant

impact on the global observation of the tides would require an immense amount of time and the interest and cooperation of other economically developed countries, especially in the southern hemisphere. There is a natural tendency to rely on the most recent computed tidal models, but our table 5 at least shows that not one of these is precise for every tidal constituent and every location, and all computational methods of dealing with the boundary dissipation are arbitrary, and dependent ultimately on local measurements such as ours. Probably the best practical compromise will be a combination of numerical solutions and measurements along strategic boundaries. For this objective, our procedure of defining the tides along linear boundaries seems better than a sparse distribution of measurements at isolated points over the globe. Extraction of tides from satellite-borne altimetry sounds an attractive possibility, but techniques of calculating the satellite's orbit seem at present to be insufficiently precise for this purpose.

The authors wish to express their gratitude to the many colleagues who have helped in various stages of this programme, particularly Peter Collar, Dennis Gaunt and Patrick Gwilliam of the I.O.S. laboratory at Wormley, Surrey, and John Huthnance and Claire MacDonald at Bidston. They are also indebted to the officers and crew of R.R.S. *Discovery* and other research vessels which have taken part, particularly Captain Michael Harding who led the majority of the Institute's tidal cruises. The work has always been funded by the U.K. Natural Environment Research Council, but during the period 1974–9 contributions were also made by the Ministry of Agriculture Fisheries and Food and by the Departments of Industry and Energy.

Appendix A. Harmonic constants from pelagic stations

The following table lists the essential details of the pelagic stations shown in figure 1 and the harmonic constants from their response analyses as described in § 5. See table 1 for the reference tide used for each station. Where a pelagic station gave two or more records from different sensors, only the best set of constants in terms of residual noise is listed, but usually all such results were very close.

The first line of each entry gives the serial code of the station, its position and depth (m), the date span (year and day number) and the record's duration in days. The second and third lines give harmonic amplitude of the tidal pressure in millibars and Greenwich phase lag in degrees, respectively, for the following order of constituents:

$$Q_1;\ O_1;\ P_1;\ K_1;\ N_2;\ M_2;\ S_2;\ K_2;\ M_3.$$

The fourth line gives estimates of the standard error of the constants quoted (from (5)) in percentage of amplitude and degrees of phase for species 1 and 2. Where these figures are bracketed, they are considered to be uncertain on account of high noise level.

Constants for relevant islands and other shore stations are listed in appendix B.

†S 14	56° 01′ N, 8° 35′ W	138 m	1970	200–224	24 d		
	2.7 7.0 2.4 8.3		22.5	112.4	42.2	12.0	1.1
	295 351 118 127		141	163	196	194	087
	7.8% 4.4°		1.2%	0.7°			
†S 13	56° 55′ N, 8° 35′ W	137 m	1970	202–231	29 d		
	2.4 6.3 2.3 8.0		21.7	109.4	41.1	11.7	0.8
	300 355 121 131		144	167	202	199	093
	7.8% 4.4°		1.0%	0.6°			
S 1	58° 02′ N, 8° 35′ W	130 m	1971	64–94	30 d		
	2.9 7.1 2.6 8.9		21.6	108.0	40.3	10.4	0.9
	311 004 122 131		156	179	212	210	088
	30.2% 17.3°		1.5%	0.9°			
S 2	58° 47′ N, 7° 30′ W	110 m	1971	61–84	23 d		
	3.1 8.2 2.9 9.9		20.8	104.0	38.9	10.1	0.9
	302 001 135 145		167	189	224	221	108
	6.6% 3.8°		1.2%	0.7°			
S 3	59° 29′ N, 6° 21′ W	188 m	1971	225–255	30 d		
	3.3 8.4 2.8 9.7		18.5	92.7	34.9	9.9	0.8
	315 012 140 150		183	205	238	236	111
	4.9% 2.8°		1.3%	0.7°			
S 4	59° 46′ N, 4° 39′ W	104 m	1971	225–235	10 d		
	3.2 8.2 2.7 9.0		16.8	83.7	31.2	8.9	1.2
	310 008 138 147		206	228	261	259	160
	11.5% 6.6°		1.7%	1.0°			
S 5	60° 00′ N, 2° 58′ W	90 m	1971	226–256	30 d		
	2.8 8.5 2.8 9.3		14.3	69.8	26.0	7.3	0.8
	326 016 138 154		232	252	287	282	147
	5.9% 3.4°		0.8%	0.4°			
‡S 7	60° 53′ N, 2° 16′ W	190 m	1972	116–122	6 d		
	2.1 6.3 2.7 9.2		11.2	56.0	21.1	5.9	0.6
	328 001 107 122		235	256	293	288	193
	(12% 7°)		1.5%	0.8°			
S 8	61° 13′ N, 0° 13′ W	156 m	1972	116–143	27 d		
	2.3 6.7 2.1 7.1		11.4	55.3	20.2	5.7	0.5
	339 026 141 156		261	283	316	311	152
	6.1% 3.5°		0.6%	0.3°			
S 10	60° 41′ N, 1° 18′ E	147 m	1972	118–145	27 d		
	1.9 5.6 1.8 5.8		10.4	50.9	18.9	5.3	0.6
	344 033 152 167		271	282	327	323	172
	7.3% 4.2°		0.6%	0.4°			
D 0	60° 11′ N, 6° 20′ W	1198 m	1973	251–279	28 d		
	2.7 7.2 2.7 9.4		14.5	72.8	27.7	7.9	0.8
	318 012 137 147		186	207	241	238	120
	5.8% 3.3°		1.4%	0.8°			
F 5	61° 29′ N, 7° 20′ W	170 m	1973	229–250	21 d		
	2.0 4.9 2.0 7.1		10.9	55.9	22.2	6.3	0.6
	328 018 134 143		175	196	229	227	117
	7.5% 4.3°		1.0%	0.6°			
F 6	62° 16′ N, 8° 30′ W	168 m	1973	228–250	22 d		
	3.4 8.4 2.4 8.2		10.2	50.9	19.6	5.6	0.5
	328 027 154 163		191	212	244	242	114
	9.0% 5.2°		1.0%	0.6°			
R 2	62° 57′ N, 10° 57′ W	444 m	1976	264–280	16 d		
	1.6 7.3 2.7 8.1		6.8	35.7	15.2	4.3	0.6
	321 038 134 144		157	177	213	212	102
	17.8% 10.2°		1.9%	1.1°			

† Collar & Cartwright (1972) referred to stations S 13, S 14 as 6, 7.
‡ S 6 (figure 1) is Foula Isle – see appendix B.

†R 3	58° 16′ N, 13° 51′ W	381 m	1977	182–263	81 d		
	2.9 7.0 2.5 8.7		16.5	83.7	32.1	9.1	0.5
	323 016 131 139		145	168	204	201	083
	4.6% 2.6°		0.3%	0.2°			
R 1	62° 50′ N, 24° 43′ W	493 m	1976	262–282	20 d		
	0.9 5.8 3.9 12.2		17.8	91.4	35.8	10.2	0.5
	021 075 129 136		157	180	217	216	215
	7.6% 4.3°		0.9%	0.5°			
D 9	60° 12′ N, 28° 46′ W	1200 m	1976	260–283	23 d		
	0.8 5.2 3.4 10.6		13.7	70.1	27.1	7.7	0.3
	003 066 130 137		160	183	222	221	256
	7.4% 4.3°		0.8%	0.5°			
D 8	57° 01′ N, 29° 58′ W	2448 m	1976	259–285	25 d		
	0.6 4.6 3.3 10.3		10.4	52.7	19.5	5.5	0.2
	002 066 133 140		152	177	217	216	289
	8.2% 4.7°		0.8%	0.5°			
D 7	53° 39′ N, 30° 10′ W	3196 m	1976	259–275	16 d		
	0.4 3.3 2.7 8.6		8.1	39.1	13.0	3.6	0.1
	347 057 129 136		132	158	198	197	297
	13.5% 7.7°		0.7%	0.4°			
D 6	53° 31′ N, 25° 06′ W	3519 m	1975	254–279	25 d		
	0.9 4.2 2.0 6.4		11.1	53.0	17.8	5.1	0.1
	330 019 142 151		123	145	183	181	135
	15.2% 8.7°		1.2%	0.7°			
D 5	53° 39′ N, 20° 00′ W	2045 m	1975	253–278	25 d		
	1.1 5.2 2.4 7.9		14.6	69.6	23.9	6.9	0.3
	315 009 136 145		120	141	177	176	010
	10.1% 5.7°		1.0%	0.6°			
C 8	53° 36′ N, 13° 51′ W	289 m	1975	250–276	26 d		
	1.8 7.3 2.8 9.0		20.6	99.1	35.2	10.2	0.7
	293 353 123 132		122	142	177	176	035
	9.5% 5.5°		1.4%	0.8°			
‡C 7	53° 37′ N, 11° 18′ W	187 m	1975	250–259	9 d		
	2.0 8.1 3.1 9.9		24.5	116.7	41.2	11.9	1.2
	280 339 106 115		125	144	179	177	013
	12.0% 6.9°		2.2%	1.2°			
C 6	50° 49′ N, 10° 55′ W	172 m	1975	249–275	26 d		
	1.9 7.1 2.4 7.6		24.1	111.8	37.1	10.7	1.1
	275 334 104 112		100	121	154	152	020
	9.7% 5.7°		1.5%	0.9°			
C 5	49° 54′ N, 10° 54′ W	190 m	1975	249–274	25 d		
	1.9 7.0 2.5 7.9		24.0	111.6	37.6	10.8	0.7
	276 335 101 110		096	116	150	148	348
	7.4% 4.3°		1.0%	0.6°			
C 4	49° 02′ N, 10° 58′ W	190 m	1975	248–272	24 d		
	2.1 7.2 2.4 7.5		23.6	109.3	36.6	10.5	0.5
	274 332 095 104		088	109	142	140	331
	9.4% 5.4°		1.3%	0.7°			
C 3	48° 37′ N, 9° 42′ W	200 m	1975	247–272	24 d		
	2.0 6.8 2.2 6.8		24.9	115.7	39.1	11.2	0.9
	271 329 093 101		087	107	140	138	345
	7.2% 4.2°		0.8%	0.5°			
C 2	48° 10′ N, 8° 20′ W	267 m	1974	307–325	18 d		
	2.3 6.6 1.7 5.5		24.4	110.5	36.2	10.4	1.3
	277 328 067 073		088	108	138	136	343
	11.2% 6.4°		3.6%	2.1°			

† Cartwright (1976*a*) quotes constants from a very short early record at a position closer to Rockall rock than R 3.
‡ For the easterly termination of line D 7, D 6, D 5, C 8, C 7 see constants for Inishbofin (appendix B).

PHILOSOPHICAL TRANSACTIONS OF THE ROYAL SOCIETY A MATHEMATICAL, PHYSICAL & ENGINEERING SCIENCES

C 1	47° 45′ N, 7° 14′ W	171 m	1973	309–342	34 d		
	2.0 6.8 2.4 7.1		28.0	129.6	44.8	12.8	1.0
	283 327 061 074		082	103	136	133	343
	3.6% 2.1°		0.7%	0.4°			
D 1	47° 27′ N, 8° 26′ W	2158 m	1974	49–84	35 d		
	2.1 7.5 2.7 7.9		26.8	122.9	42.0	12.1	1.1
	283 328 063 076		081	102	134	131	346
	6.3% 3.6°		1.1%	0.6°			
†D 1′	47° 27′ N, 8° 27′ W	2160 m	1973	310–340	30 d		
	2.0 6.9 2.5 7.4		26.5	121.9	42.2	12.0	1.0
	284 328 062 075		081	101	133	131	343
	4.6% 2.6°		0.7%	0.4°			
D 2	42° 59′ N, 10° 01′ W	3022 m	1974	310–339	29 d		
	(Amplitudes unreliable)						
	271 325 059 069		063	084	116	114	312
	13.4% 7.7°		2.2%	1.3°			
D 4	36° 55′ N, 9° 42′ W	1983 m	1975	27–56	29 d		
	1.9 7.0 2.6 7.9		22.6	100.6	32.4	9.0	0.6
	258 311 045 055		041	059	084	081	237
	18.6% 10.7°		3.2%	1.8°			
M 1	36° 41′ N, 11° 13′ W	145 m	1974	311–336	25 d		
	3.9 6.4 2.1 6.5		16.5	78.5	31.3	8.8	1.1
	270 322 051 060		042	055	077	074	(046)
	(20% 11°)		8.5%	4.9°			
M 2	36° 41′ N, 14° 15′ W	212 m	1972	198–227	29 d		
	1.5 5.6 2.0 6.0		18.8	86.3	30.6	8.5	0.2
	262 316 051 061		051	068	092	089	277
	6.2 3.6		0.8%	0.4			
D 3	37° 09′ N, 20° 05′ W	2865 m	1974	314–334	20 d		
	1.5 3.9 1.6 5.0		14.7	66.8	22.7	6.8	0.1
	246 318 058 067		048	063	083	079	325
	(15% 9°)		1.2%	0.7°			
D 10	41° 25′ N, 27° 57′ W	2432 m	1977	19–48	29 d		
	0.6 2.1 1.4 4.4		10.7	47.1	14.6	4.3	0.1
	272 342 085 094		056	073	092	089	172
	6.3% 3.6°		0.8%	0.5°			
M 4	45° 21′ N, 28° 09′ W	1047 m	1977	22–50	29 d		
	0.7 2.2 1.6 5.3		9.6	41.6	12.0	3.5	0.1
	312 010 099 107		069	089	112	109	239
	8.2% 4.7°		0.7%	0.4°			
M 3	48° 45′ N, 28° 11′ W	1153 m	1977	16–45	29 d		
	0.9 2.6 1.8 6.0		8.8	38.0	10.5	3.1	0.1
	328 026 110 119		090	112	141	139	307
	6.4% 3.7°		0.9%	0.5°			

† D 1′ is from a 'Snodgrass' capsule at practically the same position as D 1 (Unesco, 1975).

Appendix B. Harmonic constants from relevant shore stations

The following shore stations are well enough exposed to the ocean for their tidal constants to be relevant to the present work; they therefore usefully supplement the pelagic stations in appendix A. Some of the records were taken by I.O.S. as part of the present programme; their constants are not available elsewhere. Some data were obtained from other sources, where they exist, and analysed at I.O.S. to give constants that are more reliable because they are based on longer-term and more recent data than published constants from the same stations. Others are merely copied from the International Hydrographic Bureau compilation (with phase adjustment to G.M.T. where necessary), for convenience of reference.

Acronyms representing the source of the sea-level data have the following meanings: I.O.S. – Institute of Oceanographic Sciences (U.K.); D.M.I. – Danish Meteorological Institute; I.G.C. – Instituto Geodetico e Cadastral (Portugal); N.S.W. – Norges Sjøkartwerk (Norway); S.H.O. – Service Hydrographique et Océanographique de la Marine (France); I.H.S. – Icelandic Hydrographic Service; I.G.P. – Institute of Geophysics and Planetary Physics, La Jolla, California; I.H.B. – International Hydrographic Bureau, Special publication 26.

Following each name and source, the next line gives latitude, longitude, dates and duration of the data. The third and fourth lines give amplitudes H and Greenwich phases G for the same constituents as are listed in appendix A. Amplitudes are here given in centimetres of sea surface elevation, as normally for shore stations. The conversion factor to pressure in millibars is about 1.01 cm^{-1} depending on sea density and local gravity, but greater differences than 1% can be caused by coastal topography.

Hirta Island (Village Bay), St Kilda group							I.O.S.	
57° 49′ N, 8° 34′ W	1971	108–248	140 d					
2.7	7.1	2.8	9.9	21.5	107.1	40.9	11.6	0.9
298	353	122	132	150	176	210	207	080
Scolpaig Bay, North Uist, Hebrides							I.O.S.	
57° 39′ N, 7° 29′ W	1976	105–490	385 d					
1.6	3.3	1.3	4.8	23.7	119.0	44.7	12.8	1.0
297	357	077	083	155	177	211	209	089
Foula Island (Ham Voe), Shetland							I.O.S.	
60° 10′ N, 2° 03′ W	1971	132–220	88 d					
2.7	7.1	2.3	7.7	10.9	54.3	19.8	5.5	0.5
334	022	141	157	242	264	298	293	161
Baltasound, Unst, Shetland							I.O.S.	
60° 46′ N, 0° 50′ W	1972	129–245	116 d					
2.5	7.3	2.2	7.4	14.3	69.0	25.0	7.0	0.5
336	021	140	156	268	290	325	320	167
Out Skerries Island, Shetland							I.H.B.	
60° 25′ N, 0° 45′ W	1937	244–272	29 d					
—	8.2	3.4	10.1	12.5	65.8	23.2	6.4	—
—	038	150	166	280	302	333	328	—
Florø Island, Norway							N.S.W.	
61° 36′ N, 5° 02′ E	1937	282–554	372 d					
1.0	3.9	1.3	4.4	10.3	52.1	18.3	5.1	0.2
321	009	143	161	262	284	320	316	184
Sørvagur, Vaagø, Faeroe Islands							D.M.I.	
62° 04′ N, 7° 19′ W	1973	255–315	60 d					
2.2	5.3	2.4	8.5	14.0	66.5	24.8	7.1	0.5
306	014	137	145	190	211	245	242	131
Thorshavn, Strømø, Faeroe Islands							D.M.I.	
62° 01′ N, 6° 46′ W	1973	121–295	174 d					
2.4	7.2	1.6	5.1	1.9	10.3	5.4	1.6	0.7
009	050	141	143	171	198	217	213	108
Djupivogur, Iceland							I.O.S.	
64° 40′ N, 14° 17′ W	1977	168–227,	288–347	120 d				
2.8	9.2	2.2	6.6	12.7	65.2	25.5	7.2	0.6
013	061	073	077	072	097	139	139	097

Reykjavik, Iceland — I.H.S.

64° 09′ N, 21° 56′ W — 1966 — 001–1975, 360 — 3647 d

1.3	6.8	3.5	10.7		25.7	131.2	51.5	14.6	1.1
009	065	111	117		162	184	220	219	222

Angmagssalik, Greenland — D.M.I.

65° 36′ N, 37° 40′ W — 1973 — 227–249 — 22 d

1.7	7.0	4.3	13.6		19.6	101.3	39.5	11.2	0.5
023	100	143	148		179	202	248	247	267

Inishbofin I. (Bofin Harbour), Connemara, Eire — I.O.S.

53° 37′ N, 10° 13′ W — 1973 — 127–387 — 261 d

2.0	7.6	3.5	11.6		26.1	126.8	46.2	13.4	1.1
275	325	075	082		127	148	181	179	039

Port Magee (Valentia Bridge), Kerry, Eire — I.O.S.

51° 53′ N, 10° 22′ W — 1973 — 127–503 — 377 d

1.7	5.7	2.4	7.7		24.3	117.5	40.7	11.7	0.9
238	304	058	065		101	123	154	152	006

I. d'Ouessant (Lampaul), Brittany, France — S.H.M.

48° 27′ N, 5° 06′ W — 1966 — 237–434 — 196 d

1.3	5.9	2.2	6.9		41.6	206.5	82.8	20.9	1.5
275	324	073	078		089	111	150	146	030

La Coruña, Galicia, Spain — I.H.B.

43° 23′ N, 8° 23′ W — 1946 — 60–428 — 369 d

1.8	6.8	2.3	7.4		24.3	117.5	41.5	12.6	1.2
279	323	062	069		066	084	114	118	311

Cascais, Estremadura, Portugal — I.H.B.

38° 42′ N, 9° 25′ W — 1939 — 1–365 — 365 d

1.5	5.8	2.1	7.1		19.3	94.1	32.0	8.9	0.4
261	315	052	057		052	070	097	099	283

Lagos, Algarve, Portugal — I.G.C.

37° 06′ N, 8° 40′ W — 1965 — 271–1974, 261 — 3278 d

1.7	6.1	2.2	6.7		21.0	98.1	35.5	9.9	0.4
257	309	039	048		041	057	083	080	248

Madeira I. (Funchal) — I.H.B.

32° 38′ N, 16° 55 W — 1937 — 1–369 — 369 d

1.2	4.5	2.0	6.1		13.6	71.2	26.7	7.3	0.3
251	302	033	046		028	044	065	063	—

Santa Maria I. (Vila do Porto), Azores — I.H.B.

36° 57′ N, 25° 09′ W — 1975 — 207–237 — 31 d

1.1	2.9	1.1	3.4		10.9	48.4	18.9	5.1	—
257	309	057	066		053	064	084	086	—

São Miguel I. (Ponta Delgada), Azores — I.H.B.

37° 44′ N, 25° 40′ W — 1939 — 1–365 — 365 d

0.7	2.5	1.5	4.4		11.3	49.1	17.9	4.3	0.2
257	318	057	067		043	063	083	077	147

Terceira I. (Angra da Heroismo), Azores — I.G.P.

38° 39′ N, 27° 13′ W — 1957 — 185–1962, 189 — 1831 d

0.7	2.1	1.3	4.2		9.9	44.7	15.1	4.5	0.2
266	331	065	073		050	065	083	080	143

Flores I. (Lajes), Azores — I.H.B.

39° 23′ N, 31° 11′ W — 1944 — 231–259 — 29 d

—	1.0	1.0	2.0		9.0	39.0	14.0	4.0	—
—	333	081	086		041	060	080	080	—

PHILOSOPHICAL TRANSACTIONS OF THE ROYAL SOCIETY A MATHEMATICAL, PHYSICAL & ENGINEERING SCIENCES

Appendix C. A conjugate pair of filters for tidal and other purposes

The following derivation is straightforward, but from enquiries received from users of our computer program, it would seem to be useful to some workers, at least in the field of oceanography.

We wish to filter a real sequence $[x_n]$ the successive terms of which are separated in time by δt by convolutions of the form

$$\xi_n + i\eta_n = \sum_{k=-K}^{K}{}'' (F_k + iG_k)\, x_{n+k}, \tag{A 1}$$

where $''$ denotes that the end terms of the summation are halved. The sequence $[\xi_n]$ is to reproduce $[x_n]$ with part of its spectrum reduced to zero or very low amplitude but without change of 'phase', while $[\eta_n]$ is to have approximately the same spectrum as $[\xi_n]$ but with its phases advanced by $\frac{1}{2}\pi$. It follows at once from the phase requirement that

$$F_{-k} = F_k, \quad G_{-k} = -G_k \quad \text{for all} \quad k, \quad \text{and} \quad G_0 = 0.$$

Consider as a basic element of the filter $F_k + iG_k$,

$$f_k^{(m)} + ig_k^{(m)} = K^{-1} \exp(imk\Omega), \tag{A 2}$$

where $m < K$ is a positive integer and $\Omega = \pi/K$. It is well known from the theory of Fourier series that this elementary filter attenuates all of the spectrum of $[x_n]$ outside a bandwidth of angular frequency $\Omega\delta t^{-1}$ centred on $m\Omega\delta t^{-1}$ with a characteristic function approximating to

$$\sin(\omega - m\Omega\delta t^{-1})/(\omega - m\Omega\delta t^{-1}). \tag{A 3}$$

By adding the zeroth member:

$$f_k^{(0)} \equiv (2K)^{-1}, \quad g_k^{(0)} \equiv 0, \quad \text{for all} \quad k,$$

to (A 2) we sum (A 2) over $0 \leqslant m \leqslant M$, obtaining

$$F_k^{(M)} + iG_k^{(M)} = \sum_{m=0}^{M} (f_k^{(m)} + ig_k^{(m)}) = (2K)^{-1} + K^{-1} \sum_{m=1}^{M} \exp(imk\Omega). \tag{A 4}$$

Equation A 4 represents a lowpass filter the characteristic function of which is close to unity for all frequencies ω in the interval $0 \leqslant \omega \leqslant M\Omega\delta t^{-1}$ and close to zero for all $\omega \geqslant (M+1)\,\Omega\delta t^{-1}$. However, it oscillates like (A 3) close to the cut-off frequency. By a well-known principle, these oscillations are reduced to a large degree by multiplying the filter by the cosine-taper function

$$C_k = 1 + \cos k\Omega \quad \text{for all} \quad k, m. \tag{A 5}$$

On reducing the summation in (A 4) we then obtain

$$F_k^{(M)} = (2K)^{-1} C_k \sin[(M + \tfrac{1}{2})\, k\Omega]\, \operatorname{cosec}(\tfrac{1}{2}k\Omega), \; k \geqslant 1; \quad F_0^{(M)} = K^{-1}(2M+1), \tag{A 6}$$

$$G_k^{(M)} = (2K)^{-1} C_k [\sin Mk\Omega + (1 - \cos Mk\Omega) \cot(\tfrac{1}{2}k\Omega)], \tag{A 7}$$

as a good-quality lowpass filter with the characteristic properties:

close to unity for $0 \leqslant \omega \leqslant M\Omega\delta t^{-1}$;

close to zero for $\omega \geqslant (M+2)\,\Omega\delta t^{-1}$;

half-amplitude cut-off $\omega = (M+1)\,\Omega\delta t^{-1}$.

Since $C_K = 0$, the half end-terms in (A 1) may now be ignored. Choice of K sets a compromise between sharpness of cut-off and length of the convolution.

Finally,

$$F_k^{(L,\,M)} + \mathrm{i}G_k^{(L,\,M)} = (F_k^{(M)} - F_k^{(L)}) + \mathrm{i}(G_k^{(M)} - G_k^{(L)}),\ M \geqslant L+2, \tag{A 8}$$

defines a bandpass filter of similar properties with half-amplitude cut-off frequencies $(L+1)\ \Omega\delta t^{-1}$ and $(M+1)\ \Omega\delta t^{-1}$.

For the present work we have used $\delta t = 1$ h, $K = 120$, and (A 8) with the following values of L and M:

6,	12	for species 1;
14,	24	for species 2;
26,	32	for species 3.

References

Accad, Y. & Pekeris, C. L. 1978 *Phil. Trans. R. Soc. Lond.* A **290**, 235–266.
Baines, P. G. 1974 *Phil. Trans. R. Soc. Lond.* A **277**, 27–58.
Baker, T. F. 1979 *Proc. 9th G.E.O.P. conf. on applications of geodesy to geodynamics*. Ohio State Univ. 299–307.
Bogdanov, K. T., Kharkov, B. V. & Dang, Kong Min 1973 *Oceanology*, **13**, 2, 188–191.
Bowden, K. F. & Fairbairn, L. A. 1952 *Proc. R. Soc. Lond.* A **214**, 371–392.
Cartwright, D. E. 1961 *J. Inst. Navig.* **14**, 2, 130–151.
Cartwright, D. E. 1968 *Phil. Trans. R. Soc. Lond.* A **263**, 1–55.
Cartwright, D. E. 1969 *Nature, Lond.* **223**, 5209, 928–932.
Cartwright, D. E. 1971 *Phil. Trans. R. Soc. Lond.* A **270**, 603–649.
Cartwright, D. E. 1975 *Nature, Lond.* **257**, 5524, 277–280.
Cartwright, D. E. 1976*a* *Mém. Soc. r. Sci. Liège.* **6**, 10, 133–139.
Cartwright, D. E. 1976*b* *Nature, Lond.* **263**, 5574, 217–218.
Cartwright, D. E. & Edden, A. C. 1973 *Geophys. Jl R. astr. Soc.* **33**, 253–264.
Cartwright, D. E., Huthnance, J. M., Spencer, R. & Vassie, J. M. 1980 *Deep Sea Res.* (In the press.)
Cartwright, D. E., Munk, W. H. & Zetler, B. D. 1969 E.O.S., *Trans. Am. Geophys. Un.* **50**, 7, 472–477.
Cartwright, D. E. & Woods, A. J. 1963 *Dt. hydrogr. Z.* **16**, 2, 64–76.
Cartwright, D. E. & Young, C. M. 1974 *Proc. R. Soc. Lond.* A **338**, 111–128.
Collar, P. G. & Cartwright, D. E. 1972 *Deep Sea Res.* **19**, 673–689.
Collar, P. G. & Spencer, R. 1970 *Symposium on electronic eng. in ocean technology*. Inst. Electron. Radio Engrs., Lond. 341–352.
Cox, C. & Sandstrom, H. 1962 *J. Oceanogr. Soc. Japan.* 20th anniv. vol. 499–513.
Deutsche Hydrogr. Institut, Hamburg 1963 *Atlas der Gezeitenströme.* Pub. no. 2345.
Estes, R. H. 1977 *Preprint* no. X-920-77-82 (59 pp.). Goddard Space Flight Center, Greenbelt, Maryland.
Eyriès, M., Dars, M. & Erdely, L. 1964 *Cah. océanogr.* **16**, 781–798.
Filloux, J. 1971 *Deep Sea Res.* **18**, 275–284.
Flather, R. A. 1976 *Mém. Soc. r. Sci. Liège* **6**, 10, 141–164.
Garrett, C. 1975 *Deep Sea Res.* **22**, 23–25.
Gordeev, R. G., Kagan, B. A. & Polyakov, E. V. 1977 *J. phys. Oceanogr.* **7**, 2, 161–170.
Gwilliam, T. J. P 1976 *Ocean Engng* **3**, 391–401.
Hansen, W. 1948 *Dt. hydrogr. Z.* **1**, 157–163.
Hansen, W. 1966 *Mitt. Inst. Meer. Univ. Hamburg.* No. 6.
Heiskanen, W. 1921 *Ann. Acad. sci. fenn.* A **18**, 1–84.
Hendershott, M. C. 1972 *Geophys. Jl R. astr. Soc.* **29**, 389–402.
Hendershott, M. C. 1977 In *The Sea* (ed. E. D. Goldberg *et al.*), vol. 6, pp. 47–95. New York: Wiley–Interscience.
Huthnance, J. M. 1974 *Deep Sea Res.* **21**, 23–35.
Huthnance, J. M. 1975 *J. Fluid Mech.* **69**, 4, 689–704.
Huthnance, J. M. 1980*a* *Geophys. Jl R. astr. Soc.* **61**, 337–354.
Huthnance, J. M. 1980*b* *Deep Sea Res.* (In the press.)
Hyacinthe, J. L. 1974 *Conf. on 'Physics of the seas'*. Accad. naz. Lincei, Rome. **206**, 97–102.
Irish, J. D. & Snodgrass, F. E. 1972 *Am. Geophys. Un. Antarctic Res. Ser.* **19**, 101–116.
Jeffreys, H. 1920 *Phil. Trans. R. Soc. Lond.* A **221**, 239–264.
Lambeck, K. 1977 *Phil. Trans. R. Soc. Lond.* A **287**, 545–594.
Luther, D. S. & Wunsch, C. 1975 *J. phys. Oceanogr.* **5**, 2, 222–230.

PHILOSOPHICAL TRANSACTIONS OF THE ROYAL SOCIETY A MATHEMATICAL, PHYSICAL & ENGINEERING SCIENCES

Miller, G. R. 1966 *J. geophys. Res.* **71**, 2485–2489.
Munk, W. H. & Cartwright, D. E. 1966 *Phil. Trans. R. Soc. Lond.* A **259**, 533–581.
Munk, W. H., Snodgrass, F. E. & Wimbush, M. 1970 *Geophys. Fluid Dyn.* **1**, 161–235.
Parke, M. E. 1979 *Proc. 9th G.E.O.P. conf. on applications of geodesy to geodynamics.* Ohio State Univ. 289–297.
Parke, M. E. & Hendershott, M. C. 1979 *J. mar. Geodesy.* 1980 *Marine Geodesy*, **3**, 379–408.
Platzman, G. W. 1975 *J. phys. Oceanogr.* **5**, 201–221.
Proudman, J. & Doodson, A. T. 1924 *Phil. Trans. R. Soc. Lond.* A **224**, 185–219.
Robinson, I. S. 1979 *Geophys. Jl R. astr. Soc.* **56**, 159–197.
Schott, F. 1977 *Annls Géophys.* **33**, 1/2, 41–62.
Scientific Committee for Oceanic Research 1972 *Proc.* **8**, 1, 19–27.
Service Hydrogr. Océanogr. de la Marine 1968 Pub. no. 550, Paris (287 pp.)
Snodgrass, F. E. 1968 *Science, N.Y.* **162**, 78–87.
Snodgrass, F., Brown, W. & Munk, W. 1975 *J. phys. Oceanogr.* **5**, 1, 63–74.
Spencer, R. & Gwilliam, T. J. P. 1974 *Proc. Inst. elect. Electron. Engrs Conf. on Engng in ocean Envir.* **1**, 339–343.
Sündermann, J. 1977 *Dt. hydrogr. Z.* **30**, 91–101.
Taylor, G. I. 1919 *Phil. Trans. R. Soc. Lond.* A **220**, 1–93.
Unesco 1975 *Tech. Pap. mar. Sci.* no. 21, Paris. (67 pp.)
Zahel, W. 1977 *Annls Géophys.* **33**, 1/2, 31–40.
Zahel, W. 1978 (eds P. Brosche & J. Sündermann). In *Tidal friction and the Earth's rotation* (pp. 98–124). Berlin: Springer-Verlag.
Zetler, B. D. 1971 *J. phys. Oceanogr.* **1**, 34–38.
Zetler, B. D. & Munk, W. H. 1975 *J. mar. Res.* **33**, suppl. 1–13.

PHILOSOPHICAL TRANSACTIONS OF THE ROYAL SOCIETY A MATHEMATICAL, PHYSICAL & ENGINEERING SCIENCES

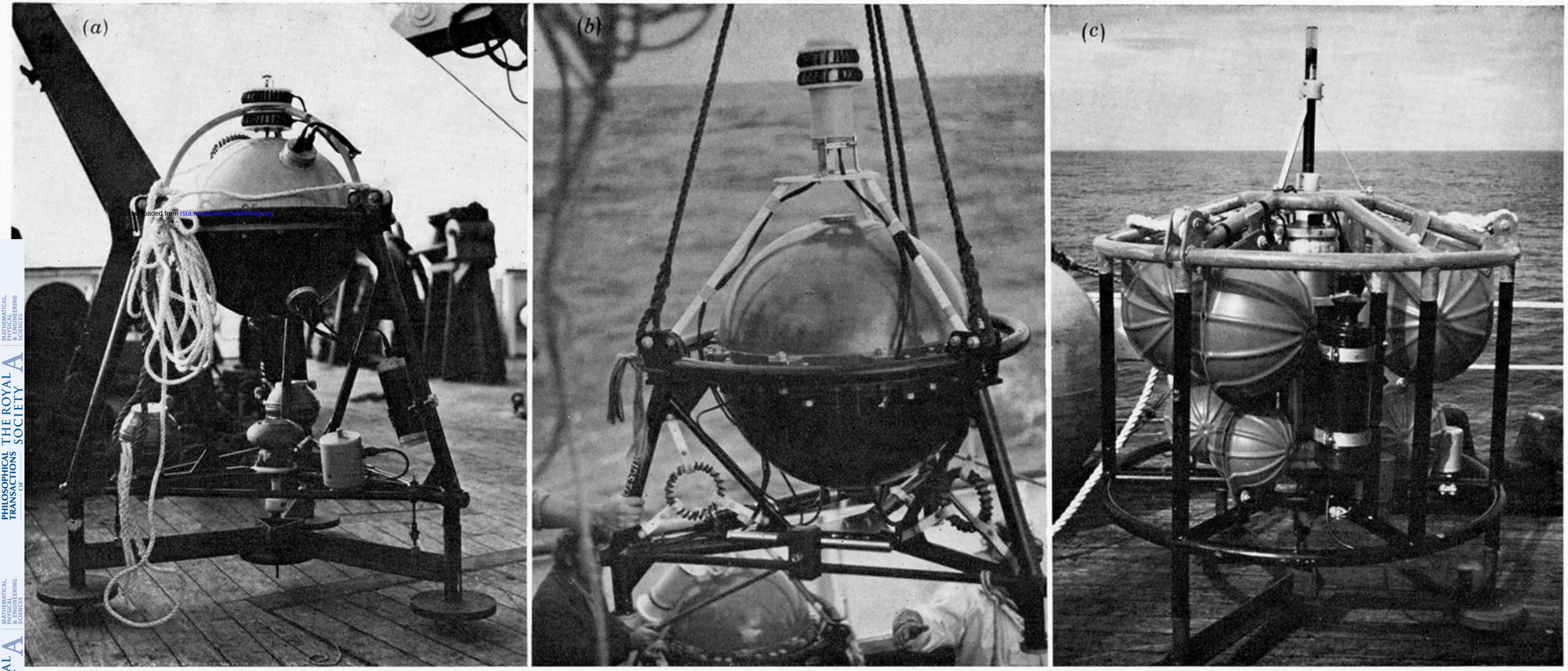

PHILOSOPHICAL TRANSACTIONS OF THE ROYAL SOCIETY A MATHEMATICAL, PHYSICAL & ENGINEERING SCIENCES

FIGURE 2. The three principal designs of sea-bed pressure capsule. (*a*) The original (mark 1) shelf tide recorder with buoyant sphere containing batteries and heavy data-logger; ellipsoidal unit near centre is capacitance-plate sensor; cylindrical unit nearby houses early strain gauge; toroidal scrolls are acoustic transducers; bottom frame is ballast attached by rapidly corrodible links (side) and acoustic/pyro-release link (centre). (*b*) 'Mark 3' deep capsule, without ballast frame when photographed. Components similar to mark 1; horizontal bar, centre, houses a quartz crystal sensor (not always included); a strain gauge unit is just visible to its left. (*c*) 'Mark 4' deep capsule with lightweight 'Seadata' cassette recorder and computer circuits inside central cylinder. Black cylinder off-centre is ceramic acoustic transducer; strain-gauge sensors are attached to the lower part of the frame; double-action release link attached centrally above ballast frame; main buoyancy provided by 'Corning' glass spheres in ribbed protective casings; the topmost cylinder is a flashing light for surface recovery at night.